UCLouvain

École polytechnique de Louvain

Multiphase model to understand the apparition of atherosclerosis

Author: **Simon YANS**
Supervisors: **Vincent LEGAT, Jonathan LAMBRECHTS**
Readers: **Michel HENRY, Evelyne VAN RUYMBEKE**
Academic year 2021–2022
Master [120] in Mechanical Engineering

Abstract

The preponderance of cardiovascular disease as the leading cause of death in the modern world has prompted the development of an accurate representation of blood flow. This is intended to provide a tool for understanding and preventing cardiovascular events. As atherosclerosis is the main pathological basis of cardiovascular events, this thesis aims to provide a first approach to understand its driving mechanisms and its development. The importance of blood platelet coagulation motivates the study of their effects on flow.

A 2D Eulerian-Lagrangian representation of the blood flow as a diluted suspension of particles is proposed with an improved description of the interactions between the particles using the non-smooth contact dynamics method. Through the implementation of a cohesive force, particle aggregation effects are reproduced in thrombus development and in the case of a stenosed artery. This work highlights the role of cohesion in the atherosclerotic event landscape, and the importance of describing flow conditions on solid phase behavior.

Acknowledgments

First, I would like to thank my supervisors Vincent Legat and Jonathan Lambrechts for their continuous support throughout this year. Their advice at each bi-weekly meeting has helped me considerably in dealing with difficulties, guiding my work, and developing critical thinking about numerical problems.

I would also like to thank Michel Henry for his truly supportive presence. His constant availability to answer my questions was precious to me, and his enthusiasm for numerical problems was really appreciated.

I would also like to thank Nathan Coppin for his pertinent remarks, questions and interest concerning my work during presentations, as well as for his help in the familiarisation with migflow software.

I thank Evelyne Van Ruymbeke for accepting to read my work.

I would like to thank my parents and friends for their supportive presence. I particularly thank my father who took the time to read and comment my work. Special thanks is also adressed to Oriane for her numerous advices.

Contents

Introduction **1**

1 Hemorheology **2**
1.1 Blood composition . . . 2
1.2 Rheology . . . 2
1.3 Constitutive blood models . . . 3
1.3.1 Non-Newtonian blood flow characterisation . . . 4
1.3.2 Newtonian blood flow characterisation . . . 4

2 The Model **7**
2.1 Migflow approach . . . 7
2.2 Non Smooth Contact Dynamics - NSCD . . . 8
2.2.1 Contact uniterality . . . 9
2.2.2 Friction modelling . . . 10
2.2.3 Time discretisation . . . 10
2.2.4 Collision resolution . . . 11
2.2.5 Impact of particle cohesion . . . 12

3 Thrombosis **13**
3.1 Introduction . . . 13
3.2 Hemostasis . . . 13
3.3 State of the art . . . 14
3.4 Numerical Results . . . 16
3.4.1 Platelets margination . . . 22
3.4.2 Impact of additional non cohesive specie . . . 23
3.4.3 Impact of the fluid . . . 24
3.5 Outcomes . . . 27

4 Stenosis **28**
4.1 Context . . . 28
4.2 Numerical Results . . . 30
4.2.1 Fluid approach . . . 30
4.2.2 Granular steady flow approach . . . 33
4.2.3 Granular pulsatile flow approach . . . 35
4.2.4 Cohesion . . . 40
4.3 Outcomes . . . 42

Conclusion **43**

Introduction

Cardiovascular diseases (CVD) are the leading worldwide cause of human mortality, with estimated near 17.9 millions annual death [Sagaro et al., 2021]. They mainly consist in disorder and physiological unbalance within the circulatory system and can consequently impact body organs. In light of its lethality, CVD prevention is a public health issue, and is extensively studied since several decades with hundreds of weekly publications. This research field is not only biomedical for *in vivo* investigations but also bio-*mechanical*. Indeed, there is a push for deeper blood flow representation to improve the understanding of blood derived-pathologies. These models increasingly include physiological parameters to enrich the variety of blood numerical representations. Particluar attention is given to models representing blood flow as a *suspension* of particles that enhance physical resolution of the fluid structure interaction. This representation provides precise information at the cellular scale such as momentum exchange.

It is now well established that CVD genesis is linked to atherosclerosis in the circulatory systems. It deteriorates blood vessel health and perturbates hemodynamics, with disastrous consequence on the vessel environment and on the downstream located organs. The vicious aspect of atherosclerosis remains in its development, which can silently begin at early stages of life and its detection often only occurs after acute cardio-vascular events.

In parallel, last decades saw the popular rise of granular flow development. Granular models allow to represent a variety of flows with a multiphasic representation. Numerical simulation of granular flows has been applied to diverse industrial and geo-physical contexts. Food processing, fluidized beds, avalanches, landslides, sediment transport, mining and milling process are examples of possible applications. This master thesis proposes a first approach to model blood flow as a dilute particle suspension in an atherosclerotic pathological context. This challenge is addressed with help of the open source software, MigFlow, whose development was motivated to provide efficient numerical simulation of such flows.

This thesis is structured in four chapters. First chapter describes the principal rheological aspects of blood and list the most well known methods commonly used for particulate blood flow modelling. Second chapter presents MigFlow and the non smooth contact dynamics method that are used in this context of multiphase blood flow modelling. Third chapter focuses on platelets behaviour within the coagulation process. The aim of the study is to verify wether a cohesive model can validate the creation of a clot over an injured area. Last chapter studies the impact of blood dynamics on flow particles. The cohesive model studied in the context of the thrombosis is then applied to the stenose, which is a larger scale case. Eventually, principal takeaways of this master thesis are discussed in the conclusion chapter, highlighting key strengths and shortfalls of the approach.

Chapter 1
Hemorheology

Hemorheology studies blood properties emanating from its components. It is now well established that a local disturbance in blood hemostatis within the circulatory system can cause pathologies with hematological origins such as leukemia, anemia, thalessemia, thrombosis, atherosclerosis, myocardial infections, hyper tension, stroke and diabetes also known as cardiovascular diseases. Mathematical and numerical hemorheology representation has consequently gained interest across the scientific community for many decades now. Their aim is to provide a more powerful representation of human blood response behaviour, and a preventive tool which is of great interest for cardiovascular prosthetic devices such as heart valves and blood pumps, clinical diagnosis and preventive therapies.

1.1 Blood composition

Blood components are divided in a fluid phase and different cell species concentrations. The first one is the plasma, which delivers the aqueous properties of blood. Plasma is mainly composed from 90-95% water and from 6-8% dissolved proteins, glucose and ionic particles (electrolytes) which have a regulatory role in the osmosis. It can also be considered as an incompressible Newtonian fluid [Pal, 2003] with temperature dependant viscosity [De Gruttola et al., 2005]. Its main role takes place in nutriment transport within the circulatory system. The second components are erythrocytes or red blood cells (RBCs), which are biconcave shaped discoïd particles with diameter $d = 6 - 8[\mu m]$. The hematocrit describes the blood RBC's volumetric content which is usually assumed to be near 45%. These cells are predominant and present specific mechanical deformable properties which will impact blood's rheological behaviour. Next component are larger ($d = 7 - 22[\mu m]$) spherical leukocytes or white blood cells, which have immunitary purposes. Last constituents are the thrombocytes or blood platelets, which are oval-shaped cell with smaller dimensions ($d = 2 - 4[\mu m]$) involved in blood clotting mechanisms.

Due to the variety of species in presence in the fluid, one can define blood as a suspension of particle of different sizes, whose properties and behaviour differs from most classical fluids.

1.2 Rheology

The particulate aspect of blood flow forces to consider the intrinsic properties of those particles. Determining the rheology of such a complex mixture is no trivial task. First of all, all cells in presence have surface charges inducing diverse interaction mechanisms with fluid phase, other blood cells or with endothelial cells that form the internal layer of the vessel wall. Those mechanisms can still be approximated by basic particle-particle forces such as Van der Waals (vDW)-London forces or Coulombic forces. Well described blood rheology can significantly enhance numerical simulations results and comprehension. This section focuses on the the main blood rheological aspects.

Attention is given to the RBCs given their predominant presence in the suspension. Their membrane is composed of a thin elastic lipid bi-layer, and enclose the Newtonian hemoglobin fluid. RBCs membrane exhibit elastic and deformable properties allowing them to aggregate depending on the flow conditions and the level of blood concentrations in fibrinogen and globulins, that can be seen respectively as cohesive molecules and cell transmitters. At low shear rates, those RBCs form a 3D branched structure and over a specific time duration aggregate. At high shear rates, aggregates are torn apart and get suspended in plasma where they form the so called "rouleaux", with RBCs content inversely proportional to shear rate [Fung, 1993]. One understands that transient RBCs interactions are shear rate dependant and are at the origin of the non-Newtonian characterisation of blood flow. Induced non-Newtonian effects are manifested through different phenomenons:

Shear thinning Blood has the tendency to decrease its viscosity with increasing shear stress when RBCs deform and align with the flow [In and Kang, 2002]. This effect is further accentuated due to its hematocrit dependance. At the opposite, viscosity is increased with decreasing shear rate favoring RBCs interactions. This effect has been extensively investigated in vitro by [Chien, 1970].

Visco-elasticity results on the one hand from the elastic energy storage emanating form RBCs reversible deformability occurring over a relaxation time proper to the cell membrane, and the rate of dissipation of energy due to cell interactions and membrane relaxation on the other. [Thurston, 1973] has experimentally put forward the dependance of the RBC's relaxation time to the shear rate and showed that the viscoelastic nature of blood is less prominent at high shear rates and more prone to occur in small vessels, under pulsatile conditions. In pulsatile flow regime, visco-elasticity induces a phase lag between the shear rate and the shear stress.

Thixotropy is associated to the non-instantaneous buildups and breakdown of the RBCs's formation due to Brownian motion, the elongation and relaxiation time of RBCs and allows to describe the transient aspect of blood flow. Most thixotropic models account for *(i)* the visco-elasticity of individual cell, *(ii)* the total visco-elastic stress contribution from rouleaux and *(iii)* the temporal dependence of rouleaux micro-structure to shear rupture and shear aggregation.

Yield stress fluid : if no flow is applied, inter particular aggregation occurs between blood cells, blood plasma and endothelial cells. As a result, the blood requires a finite stress to start flowing. Yield stress is not constant over time thus thixotropic. Note that if the suspension is continuously sheared, the hydrodynamic forces overcome the linking forces between blood components, which translates in a shear thinning of the supsension.

1.3 Constitutive blood models

Multiple constitutive models have been derived in the last decades to describe the variety of physicals blood aspects.

1.3.1 Non-Newtonian blood flow characterisation

Shear thinning and yield stress effects are well captured through generalised non-Newtonian models. The most well known viscosity model is the power-law model fitted for blood by [Liepsch and Moravec, 1984]. Herschley Model included shear stress influence on viscosity. The notable Casson model initially proposed for ink in 1959 later relates blood viscosity to shear rate, shear stress and infinite shear viscosity. This model suffered from non physical behaviour at low shear stresses. Multiple works have resulted in the introduction of relevant physological parameters in the Casson model. The parametrisation proposed by [Apostolidis and Beris, 2014] for yield stress and Casson viscosity take in account the temperature, the hematocrit and the fibrinogen concentration.

This category of generalized constitutive model experiences difficulties to describe visco-elastic or thixotropic effects of blood under pulsed conditions, hence visco-elastic model are investigated. Earlier models for visco-elsaticity were based on a simple Maxwell model, later improved by Oldroyd B fluid model. According to shear dependent relaxation time of RBCs observed by [Thurston, 1973], [Anand and Rajagopal, 2004] proposed a generalised version of Oldroyd-B shear-thinning viscoelsatic model, providing the best fit with rheological experimental data in both steady and pulsatile conditions. [Anand et al., 2013] later extended this method for 3D complex geometries.

1.3.2 Newtonian blood flow characterisation

As consequence of the shear thinning effect, blood behaves as Newtonian fluid with constant viscosity over a certain shear rate that depends on hematocrit, hence blood can be described with Newtonian assumption under certain conditions. Several hematocrit dependent viscosity models based on the Einstein experience of dilute monodispersed spheres [Haines and Mazzucato, 2011] are available in the litterature. Reformed version such as [Phillips et al., 1992] model account for large particle volume fraction (up to 70%) and for the impact of shear induced particle migration. [Womersley, 1955]was the first to introduce an analytical resolution for oscillatory pressure driven blood flow under Newtonian assumption.

They are other specific conditions that can legitimate the Newtonian assumption: [Cho and Kensey, 1991] state that non-Newtonian effect of blood viscosity must be considered in steady conditions for flow with Reynolds $Re \leq 60$, based on wall shear stress and pressure drop observations.

Numerous numerical methods have been developed in the recent past years to describe blood behaviour originating from its particular aspect. This sections presents the most widely used methods to describe blood being modelled as an heterogeneous suspension of plasma and blood particles such as RBCs.

Dissipative Particle Dynamics - DPD Introduced by [Hoogerbrugge and Koelman, 1992], each particle population represent a component of the flow (fluid,membrane,wall boundary). It originates from molecular dynamics since particle motion follows Newton's second law. Conservative, dissipative and random forces equations characterise DPD parti-

cles interactions. Studies from [Fedosov et al., 2014] and [Tosenberger et al., 2011]describe RBCs behaviour in different flow conditions and study their deformation and interaction schemes. Coarse particle is encouraged for RBC membrane modelling since DPD particles mass must be decreased accordingly and thus requires very small time steps for sake of numerical stability, increasing computational cost.

Smoothed particle hydrodynamics - SPH Originally introduced by [Lucy, 1977], [Gingold and Monaghan, 1977] for astrophysical applications, SPH discretizes the computational method into a set of particles based on a Lagrangian interpolation of the Navier-Stokes equations. SPH-particles properties are interpolated from neighboring particles using a smoothing kernel function. [Hosseini and Feng, 2009] studied RBCs deformation through a stenosed canal, and [Tanaka and Takano, 2005] studied RBC migration through a plasma-RBC suspension. Due to the dependence of the solution to the smoothing kernel radius, instabilities and loss of solution accuracy may be experienced at the boundary conditions, whose implementation are delicate although alternative fixes exist (mirror particle, periodic boundaries, force imposition, fixed particle with extrapolating velocity). Despite its visual advantage, this method does not accurately capture the physics of the problem.

Immersed boundary method - IBM proposed by [Peskin, 1972]in a cardiovascular context is a fluid-structure interaction model using an Eulerian-Lagrangian representation respectively for the fluid and an immersed membrane. This method is useful to characterise large solid deformations, particle membrane being modeled as a set of connected particles. Both scales are linked together with a Dirac smoothing function that translates the Lagrangian membrane forces to the Eulerian nodes of the fluid phase governed by Navier-Stokes equations. Solid phase interaction forces are expressed in a source term of the fluid governing equation solved over the domain. Nevertheless, the use of a smoothing function can impacts method stability and solution accuracy on boundaries [Hashemi, 2018].

Lattice Boltzman method - LBM Detailed by [Chen and Doolen, 1998], LBM is a statistical physics method. The fluid is discretized as a set of fictitious interacting particles evolving on a discrete regular lattice. LBM is based on the Boltzmann equation instead of classical incompressible Navier-Stokes (NS) equation. NS formulation can be retrieved from the Chapman-Enskog expansion under low Mach number assumption, thus only considering weakly compressible flows. Each lattice node is associated with 9 directions (in 2D) corresponding to probability distribution functions that evolve given particles interactions. Quantities of interest are interpolated from those distributions. Although this method does not provide convenient error analysis , it provides a quick and versatile method for parameter sensitivity analysis, preceding more precise computational method such as the finite element method [Weichert et al., 2013]. This method is also more computationally intensive and requires parallel computing architecture, and imposed regular lattice does note make the method suitable for complex geometries.

IBM are commonly coupled with LBM, influence of additional deformable membrane forces can be added by communicating the force density experienced by the fluid at the Eulerian nodes as a source term in the LBM formulation. This method coupling is very prone to the study of the rheological impact of RBCs on the blood behaviour. [Zhang et al., 2008] studied their desagregation through stenosed vessel with an LBM-IBM approach.

One understands that special attention is given to the particulate aspect of blood flow modelling. No continuous approach is considered here, which is not surprising in this case given the important impact of RBCs on the blood rheology. The limitations of DPD, SPH, and IBM methods due to the use of a smoothing function encourages to consider an enhanced description for particle interactions.

To this use, the **Discrete Element Method - DEM** developped by [Cundall and Strack, 1979] is a suitable approach. It provides a better description for grain trajectories and grain interaction forces through contact law implementations with contact detection methods. DEM mainly considers rigid particles, which may be discouraging regarding RBCs deformability. However, it can still provide pertinent framework by assuming constant RBCs geometry given flow properties and by considering other blood constituents such as white blood cells or platelets, less prone to deformations. Due to the continuum aspect of the fluid phase, Eulerian representation is preferred to the Lagrangian particulate fluid representation in DPD and SPH methods. Furthermore, unresolved computational fluid dynamics (CFD) method can reduce computational cost by a coarse representation of the fluid phase compared to the representation of the particle scale. This can be achieved through the **Finite Element Methods - FEM**, taking advantage of the method flexibility in term of fluid description and its handling of complex geometries. Given appropriate closure of the model, a CFD-DEM method can be applied to the study of blood as a dilute suspension of blood constituents, hence modelling its non Newtonian behaviour. The latter is presented in the next chapter.

Chapter 2
The Model

2.1 Migflow approach

An immersed granular flow numerical simulation of platelets aggregation is performed using the opensource multiscale unresolved CFD-DEM model MigFlow® software. The approach is based on a Lagrangian-Eulerian representation of the fluid-grain mixture. The granular phase is described in Lagrangian coordinates with the discrete element method. The fluid phase is computed at a coarser scale than the granular scale by averaging Navier-Stokes equations over a finite control volume element bigger than the grain size with a Finite Element Method. The fluid integral over the element is approximated by its mean and multiplied by the fluid volume fraction over the element: the porosity ϕ, allowing lower computational cost compared to fully resolved methods that describe fluid flow on a smaller than the particle size. The locally averaged equations of motion have been derived by [Anderson and Jackson, 1967]. Assuming fluid incompressibility and defining $\mathbf{u} = \phi\mathbf{w}$ as the volume averaged fluid velocity $\mathbf{w}$, [Constant et al., 2018] express the system mass and momentum conservation equations of the fluid phase of the granular flow as:

$$\frac{\partial \phi}{\partial t} + \nabla \cdot \mathbf{u} = 0,$$

$$\rho \left[\frac{\partial \mathbf{u}}{\partial t} + \nabla \cdot \frac{\mathbf{u}\mathbf{u}}{\phi} \right] = \nabla \cdot [2\mu\phi\mathbf{d}(\mathbf{u}) - p\mathbf{I}] + \mathbf{f} + \phi g\mathbf{g}.$$

where μ is the fluid viscosity, p is the pressure, $\mathbf{I}$ is the identity tensor, $\mathbf{f}$ is the fluid-grain interaction forces and $\mathbf{g}$ is the gravity. Gravitational effects are assumed to have negligible impact on the particle flow in this case. $\mathbf{d}(\mathbf{u})$ is the deformation rate tensor of the fluid, the symmetric part of the strain rate tensor. With the introduction of porosity, it is defined as:

$$\mathbf{d}(\mathbf{u}) = \frac{1}{2}\left(\nabla \frac{\mathbf{u}}{\phi} + \left(\nabla \frac{\mathbf{u}}{\phi} \right)^T \right).$$

The discrete nature of granular phase is captured through a Lagrangian representation, providing trajectories and forces applied on each grain. Particles dynamics are described according to Newton's second law of motion, providing grain velocities:

$$\frac{d}{dt}(m_i \mathbf{v_i}) = m_i \mathbf{g} - V_i \nabla p|_{\mathbf{x}_i} - \mathbf{f}_i,$$

where $\mathbf{f}_i$ is the fluid-grain interaction force, or drag contribution. The second term accounts for the pressure gradient contribution. Particles parameters $\mathbf{m_i}$, $\mathbf{v_i}$,V_i and $\mathbf{x_i}$ describe respectively particle mass, velocity, volume and position. Contact interactive forces are obtained with non smooth contact dynamics (NSCD) method described in the next section. Model closure is achieved through a coupling between both phases. Direct momentum transfer

between phases cannot be achieved since the fluid phase is not properly described at the granular scale. Here, a coupling term is used and based on the pressure gradient as well as on the drag contribution of the fluid to a single grain, pondered by an independent function of the local porosity to account for neighbouring grains influence.

2.2 Non Smooth Contact Dynamics - NSCD

In order to compute grain interactions forces, particle contacts are solved through the non smooth contact dynamics method. Grains being considered as isolated bodies, their behaviour is described by dynamic equations and considers their interactions as external forces. The NSCD approach as described by [Jean, 1999] is interesting due to its fully *implicit* nature compared to smooth methods that are explicit, consequently taking advantages of greater time steps, and prohibits particle inter-penetrations due to superimposed corrections on grain velocities that are prone to interaction.

The NSCD method is based on the monitoring of a set of *contact points*. A contact point is created when two particles are susceptible to collide. For sake of computational efficiency, a contact is only created when the distance between potential contact points C_A and C_B (as depicted in Figure 2.1) is smaller than an imposed distance that, in this case, is fixed to the grain radius. The method solves iteratively contacts between particles occurring given a prescribed time interval Δt, computing configuration and speed values $(\mathbf{q}, \mathbf{u})$ from the last ones, avoiding particle interpenetration and thereby suppressing possible oscillations due to stiff response observable in smooth methods.

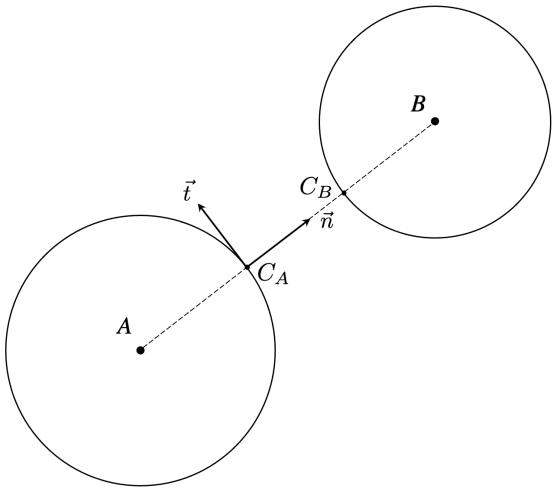

Figure 2.1: Antagonist particle A colliding with candidate particle B

The variables of interest in a friction contact are the coordinates $\mathbf{x} = (q_1, q_2, q_3)$ of each particle's center of gravity in the global frame as well as the components of the rotation vector of the particles $\omega = (q_4, q_5, q_6)$, usually described with Euler angles. Those values are included in a configuration vector q:

$$\mathbf{q} = \begin{pmatrix} \dots & \mathbf{x_i} & \theta_\mathbf{i} & \mathbf{x_j} & \theta_\mathbf{j} & \dots \end{pmatrix}^T$$

Equations of motion for a set of particles are described with Newton's second law, which takes the following form:

$$\mathbf{M}(\mathbf{q})\frac{d\mathbf{u}}{dt} = \mathbf{F}(\mathbf{q}, \dot{\mathbf{q}}) + \mathbf{E} + \mathbf{r}$$
$$\mathbf{q}(t) = \mathbf{q}(\tau) + \int_{\tau}^{t} \mathbf{u} dt$$

With $\mathbf{M}$ the mass matrix, $\mathbf{F}$ the quadratic acceleration terms, $\mathbf{E}$ the explicitly known forces and $\mathbf{r}$ the generalized contact forces induced by other particles in the current configuration. Contact tangential and normal force components are expressed in the local frame $(\vec{t}, \vec{n})$ and are respectively noted $\mathbf{R_T}$ and $\mathbf{R_N}$. One also defines for all contact points the *relative* speed vector U as the velocity difference between the candidate and the antagonist corpse described in figure 2.1:

$$\mathbf{U} = \mathbf{v}_B|_{contact} - \mathbf{v}_A|_{contact}.$$

The tangential component $\mathbf{U_T}$ of this quantity represents the sliding velocity. The normal component $\mathbf{U_N}$ is interpreted as an image of the normal distance between potential contacting particles.

In compact population of particles one should expect numerous shocks or at least speed discontinuities. Velocity functions with locally bounded variations are considered to ensure mathematical robustness. That is, the speed function has one upper limit $u(t)^+$ and one lower limit $u(t)^-$, and $u(t)^- = u(t) = u(t)^+$ when the function is continuous.

2.2.1 Contact uniterality

In this method, the uniterality of the interaction between particles ensures no interpenetration. This condition is satisfied by imposing a positive distance between them:

$$g(t) = ||\mathbf{x_j} - \mathbf{x_i}|| - (r_i + r_j) \geq 0 \qquad \frac{d}{dt}\left(g(t)\right) = U_N$$

The latter is satisfied if the normal component of the reaction force R_N exerted by the antagonist on the candidate is positive and null when contact ceases since no cohesion is yet considered. Those conditions translates the Signorini condition expressed with respect to the distance gap between colliding particles:

$$g(t) \geq 0, \qquad \mathbf{R_N}(t) \geq 0, \qquad g(t)\mathbf{R_N}(t) = 0$$

Considering smooth displacements and since the distance function g(t) is continuous, problem might happen if a shock occurs at instant t. The use of function with locally bounded variations allows to write the Signorini condition as a function of speed:

$$\mathbf{U_N}(t)^+ \geq 0, \qquad \mathbf{R_N}(t) \geq 0, \qquad \mathbf{U_N}(t)^+\mathbf{R_N}(t) = 0.$$

Uniterality of motion is however non sufficient to determine particle motion. When one considers particle percussions, that occurs on a far more smaller time scale, complicated effects may appear such as deformations. A supplementary behavioural law is used to compute

the post percussion resulting velocity. Newton shock law gives the resulting velocity as function of a restitution coefficient $k \in [0,1]$ such that $U_N^+ = -kU_N^-$. Zero restitution coefficient is chosen in this case, corresponding to inelastic collisions, that present useful energy dissipating properties that avoid the use of a damping Voigt model. Nevertheless it sufficiently describe the particle population physics, thus $U_N^+ = 0$.

2.2.2 Friction modelling

Dry friction is modelled with a Coulomb law. Resulting tangential force induces sliding opposed to the sliding velocity. This tangential force is bounded, proportional to the normal force $\mathbf{R_N}$ and pondered with a friction coefficient μ:

$$||\mathbf{R_T}|| \leq \mu \mathbf{R_T} \qquad ||\mathbf{U}(t)^+|| \neq 0 \implies \mathbf{R_T} = -\mu \mathbf{R_N} \frac{\mathbf{U_T}^+}{||\mathbf{U_T}^+||}$$

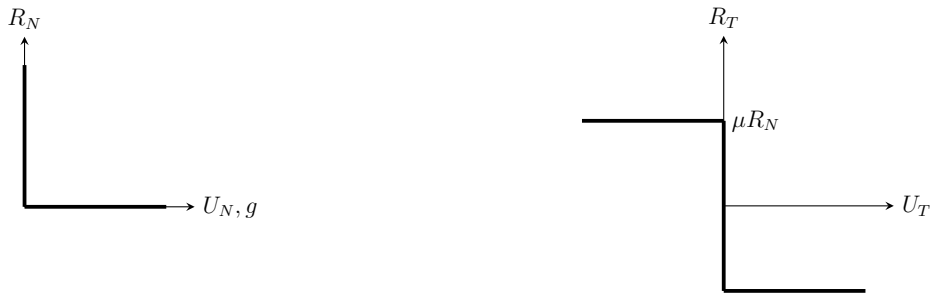

(a) Signorini condition (b) Coulomb law

Figure 2.2: Graphic representations of contact uniterality and friction law as functions of the components of the relative contact speed U_N and U_T

Since contacts are described in the local frame of reference $(\vec{t}, \vec{n})$ of the couple of contacting particles, an application $\mathbf{H}^*$ is used to switch from global to local frames:

$$\mathbf{U} = \mathbf{H}^*(\mathbf{x})\mathbf{u}$$

2.2.3 Time discretisation

A two dimensional case with a collection of spherical particles is considered such as the mass matrix $\mathbf{M(q)}$ is constant with null quadratic acceleration terms. The only known forces at time t are provided by the fluid phase. The system becomes, using an implicit Euler method:

$$\mathbf{M}\left(\mathbf{u}^{(i+1)} - \mathbf{u}^{(i)}\right) = \mathbf{E}^{(i,i+1)} + \mathbf{p}^{(i+1)},$$
$$\mathbf{q}^{(i+1)} = \mathbf{q}^{(i)} + h.\mathbf{u}^{(i+1)},$$

unknowns being the impulsion $\mathbf{p}^{(i+1)}$ sum of all impulses originating from experienced contacts during the time step h by the particle and the approximation of the right limit of the speed at the end of the time step.

2.2.4 Collision resolution

Since uniterality of Signorini condition and Coulomb law are multi-applications, one cannot derive a single ordinary differential equation taking in account dynamics, uniterality, shocks and friction. If two disks D_i, D_j with speeds u_i, u_j collide:

$$g = 0 \qquad \mathbf{U_N}^- \leq 0 \qquad \mathbf{U_N}^+ = k\mathbf{U_N}^- \qquad \mathbf{R_N} \geq 0$$

Defining:

$$\mathbf{W} = \mathbf{H}^*\mathbf{M}^{-1}\mathbf{H} = \begin{pmatrix} \mathbf{W_{TT}} & \mathbf{W_{TN}} \\ \mathbf{W_{NT}} & \mathbf{W_{NN}} \end{pmatrix}$$

where

$$\mathbf{W_{TT}}_{ij} = m_i^{-1} + m_j^{-1} + I_i^{-1}r_i^2 + I_j^{-1}r_j^2$$
$$\mathbf{W_{NN}}_{ij} = m_i^{-1} + m_j^{-1}$$

$\mathbf{W_{TN}}, \mathbf{W_{NT}}$ are null in case of disks, but not with complex forms.

Transitioning to local frame of reference, the equation of dynamics for the candidate are:

$$\mathbf{H}^*\mathbf{u}^+ = \mathbf{H}^*\mathbf{u}^- + \mathbf{H}^*\mathbf{M}^{-1}\mathbf{H}\mathbf{P}$$
$$\mathbf{U}^+ = \mathbf{U}^- + \mathbf{W}\mathbf{P}$$

More globally,

$$\mathbf{U^{i+1}} = \mathbf{U_{free}} + \mathbf{W}\mathbf{P^{i+1}}$$

Where $\mathbf{U_{free}}$ is the value taken by the relative speed $\mathbf{U^{i+1}}$ when all friction reactions involved in the contact are null ($\mathbf{P} = 0$). Decomposing for normal and tangential components:

$$\mathbf{U_N^{i+1}} = \mathbf{U_{freeN}} + \mathbf{W}\mathbf{P_N^{i+1}}$$
$$\mathbf{U_T^{i+1}} = \mathbf{U_{freeT}} + \mathbf{W}\mathbf{P_T^{i+1}}$$

This problem is known as the Signiorini μ-Coulomb standard, and has unique solution under reserve that dynamic bowing is exluded. This is ensured as long as :

$$-1 < -\mu\frac{\mathbf{W_{NT}}}{\mathbf{W_{NN}}} < 1,$$

which is always the case of disks since $\mathbf{W_{NT}} = 0$. Recalling the zero restituion coefficient implying $U_N^{i+1} = 0$ and defining $\mathbf{P_{stick}} = -\mathbf{W_{TT}^{-1}}\mathbf{U_{freeloc,T}}$ as the impulse canceling the tangential relative velocity, the force impulse over the time step is then calculated as:

$$\mathbf{P_N^{i+1}} = -\mathbf{U_{free,N}}/\mathbf{W_{NN}}$$
$$\mathbf{P_T^{i+1}} = \mathbf{min}(\mu{\mathbf{P_N}}^{i+1}, ||\mathbf{P_{stick}}||)\frac{\mathbf{P_{stick}}}{||\mathbf{P_{stick}}||}$$

2.2.5 Impact of particle cohesion

Cohesive inter-particular interaction force is efficiently implemented into to the NSCD method. When an arbitrary cohesive force F_{cohes} is applied to the contact, its effect is expressed as an additional external induced velocity, normal to the local contact frame of reference:

$$\mathbf{U}_{cohes} = \mathbf{W_{NN}} \cdot \mathbf{F_{cohes}} \cdot h.$$

We also know that the NSCD method limits over the time step the displacement of a grain by an arbitrary fixed distance. The latter is here chosen as the distance between the two contact points, the distance function g. The normal speed condition for the cohesion to be applied at each contact is then given by:

$$\mathbf{U_N} + \mathbf{U}_{cohes} \leq \frac{g}{dt}.$$

The local variation of the relative contact speed is straightforward:

$$\delta\mathbf{U_N} = \mathbf{U_N} - \mathbf{min}\left(\mathbf{U_N} + \mathbf{U}_{cohes}, \frac{g}{h}\right).$$

Note that the implementation of a cohesive force between particles is easy to implement into the contact solver. The difficult part being the conception and choice of the cohesive force itself.

Chapter 3
Thrombosis

3.1 Introduction

Thrombosis is a blood disease, which prevents the dis-aggregation of coagulation products with various origins and risk factors. It occurs when the balance between pro-coagulants and anti-coagulants is impaired [Furie and Furie, 2008]. This results mainly in an obstruction of the lumen (vessel internal cross section) that may imply hazardous complications. The coagulation products result from blood hemostasis, forming a blood clot near an injured or damaged area. This chapter provides a phenomenological model for thrombus formation. To this use, a cohesive model is described and implemented to mimic aggregation and rupture patterns of the blood platelets.

3.2 Hemostasis

Hemostasis is a response to injury process that designates the set of phenomena that prevents blood losses and physiologically restores the blood vessel. The major part of this process concerns blood coagulation to keep the high pressure flow within the circulatory system when the blood vessel is damaged. The injury site is covered with a fibrous structure of blood agglomerates that locally affects hemodynamics. The cap remains until the wound is healed and dissolves afterwards. Blood platelets are of main interest since they are at the heart of the coagulation process. They dispose of a large number of membrane receptors that participate to their interaction with the wall, other platelets or coagulation factors [Reyes Gil, 2019].

Vasoconstriction of the blood vessel is the first response to the injury. The lumen is reduced, minimizing blood losses and also enhancing the reactivity of the hemostasis subprocesses. It is followed by a primary hemostasis phase, its main goal being the formation of a platelet plug over the injury by platelets aggregation. Platelets aggregation and activation have two origins [Furie and Furie, 2008]. The first one is collagen related: the von Willebrand Factor (vWF) present in blood fixes to the endommaged entdothelial cells with exposed collagen. The bounding of fixed vWF with the platelets receptor gylcoprotein (GP) Ib promotes platelets *aggregation*, while the exposed collagen preferentially bounds with GPVI platelet receptor. The collagen bounding triggers platelets *activation* that favorizes agglomeration. The second pathway is related to tissues (endothelial) factors such as thrombin: the activation of coagulation factor VIIa and IXa generates thrombin that activates platelets by affinity with the Par1 platelet receptor. Activated platelets undergo change of geometry from ovoid to stellar, and start diffusing granular contents. Those particles have different impacts. Their population is mainly composed of the so called alpha-granules, storing vWF , fibrinogen matrix proteins and dense granules containing adenosine tri/diphosphate (ADP,ATP). This influences the platelets activation response. The released particles activate other platelets in turn and change the conformation of the GPIIb/IIIa platelets receptor, tremendously enhancing the platelets affinity to ligants. This amplifies the aggregation and activation process

of platelets forming the clot over the injured area. A secondary hemostasis then occurs, principally aiming at the production of fibrin from fibrinogen. The latter mainly originates from blood (production in the liver), or from released alpha particles. The wide amount of coagulation factors involved in this process is complex, and is known as the coagulation cascade. However, it can be resumed in a two phase process. At first, thrombine is used to cleave fibrinopeptides of the fibrinogen to form fibrine monomers. Then, the obtained momoners is polymerized into a three dimensionnal fibrine network. The plasma transglutaminase factor FXIIIa intiates cross-linking of these three-dimensional fibrine polymers, consolidating and stabilizing the formed clot [Weisel and Litvinov, 2017]. A final tertiary hemostasis initiates fibrinolysis that dissolves the fibrin bounding wihtin the clot once the wound is healed. Fibrinolysis starts with the release of the tissue plasminogen activator (t-Pa) by the healing endothelial cells. t-Pa activates the inactive plasmine (plasminogen) intially present in blood and regulated by the liver. Plasmine is then responsible for the clot lysis, [Chapin and Hajjar, 2015], leaving a restored endothelial.

Thrombosis originates from dysfunctional hemostasis, with various risk factors such as genetics, cancer, obesity, or lack of physical activity [Cushman, 2007].

3.3 State of the art

Numerical methods are important to develop the understanding of the clot formation with its complex processes. Exact modelling seems out of reach, if one has to consider every involved species with appropriate concentrations and to model their behaviour and their interaction with other species. This would also require extensive biochemical, chemo-mechanical and bio-mechanical knowledge that do not prevail at this stage of work. Naturally, enormous computational challenges are also expected to model platelet adhesion, aggregation and activation, or fibrin production through the coagulation cascade with underlying reactions. The scale disparity of the implicated components also sets difficulties to capture and correlate the information. Hence a more rational approach is to be considered. Here attention is set on platelets and the flow, whose disturbances and effects impact platelets behaviour. Several numerical models are proposed in the literature to study the interactions between blood platelets.

[Fogelson, 1984] firstly described the interaction effects of fluid and platelets aggregation in small arteries with a discrete and later continuum [Fogelson, 1992] model. Both are based on an Eulerian approach for the fluid, described by Stokes or Navier-Stokes equation. Platelets cohesion is modeled by solving advection-diffusion-reaction equation for the concentration of the coagulation factor ADP and a fictious fluid-dynamics body force was introduced to reproduce flow disturbances due to the thrombus.

More recently, [Leiderman and Fogelson, 2011, 2013] proposed a very complete continuous spatial-temporal coagulation model. It accounts for a tremendous amount of bio-chemical factors to describe the coagulation bio-chemistry, chemical activation and deposition of blood platelets and the fluid-platelet interaction. To enhance fluid description where platelets aggregate and link together within the thrombus, a porosity function is introduced. This study

considers the thrombus as a porous media, thus providing a porosity function, and demonstrates the growth dependence to wall shear stress and near-wall platelets excess.

The main drawback of such methods is that it assumes the blood flow to be homogeneous and does not account for the influence of individual blood components. Efforts were later made to include an enhanced description of the fluid-structure interaction and cellular-level information. This improves flow description in complex geometry cases: continuum models being unable to model flow obstruction due to particles in narrow geometry. Such models allowed to track displacements and interaction between individual platelets modelled as discrete elements. The fluid platelet interaction gave birth to numerous models using different approaches.

[Pivkin et al., 2006] proposed a thrombus formation model based on the force coupling method. Delayed platelet activation is modelled with an activation distance w.r.t injured area. The attractive-repulsive particle interaction is modeled with a potential-derived force, which is linearly dependent on the distance. The repulsion avoids particle contact resolution. The results reproduced the experimental observations performed in vivo by [Begent and Born, 1970].

[Fogelson and Guy, 2008] studied platelets aggregation in a microscopic model using the IBM. The model individually tracks particles, the platelet-platelet, platelet-fluid, platelet-wall interactions, and expresses platelet activation as a function of concentration of chemical activators. Bounded non physical oscillations appear due to the nature of the IBM. Moreover, the results highlights the importance of the porosity to accurately model platelet aggregates.

[Xu et al., 2008] also proposed a discrete multi-scale model based on the cellular Potts methods. It combines a discrete description of platelets and additionnal blood cells, while coagulation reaction kinematics and blood flow hydrodynamics are continuously described with partial differential equations.

Particle method were also used by [Kamada et al., 2010] by modelling platelets-wall adhesion with a mechanical spring force. Thrombus formation was investigated under different flow regimes highlighted the importance of flow conditions in thrombus growth. [Mori et al., 2008] extended particle interaction to two plasma particle species: vWF and fibrinogen using two calibrated Voigt models. Completed fibrinogen-plasma-platelet simulation was performed using Stokesian dynamics. [Tosenberger et al., 2013] described thrombus growth with a DPD method. Each DPD particle represent a volume fraction of the medium instead of a single particle. DPD particles are used for the fluid phase and for individual platelets. Coagulation with platelets aggregation is controlled via a simplified reaction diffusion-advection-equation modelling fibrin concentration.

[Yazdani et al., 2017] proposed a shear dependent platelet adhesive model based on the work of [Pivkin et al., 2006]. Platelets interactions were described using a Morse potential and validated for a large range of shear rates. Platelet aggregation was coupled to a coagulation cascade leading to fibrin formation. This model is based in a Eulerian-Lagrangian

framework. Although yielding satisfying results, the method avoids contact resolution by assuming particle repulsion.

As previously observed in Chapter 1, there is a push for an enhanced *particulate* description of blood. Continuum models do not propose such description of the flow, and are discarded in favor of particulate methods. Limitations of particulate methods such as DPD or IBM were previously explicited, and Eulerian-Lagrangian models are preferred. Once again, the MigFlow model stands out for its enhanced description of particles with the concept of the porosity and contact resolution, which seems to be a grey area for certain methods that rather use particle repulsion to avoid contact handling.

3.4 Numerical Results

As seen in previous section, thrombus formation and growth is physically described by a numerous variety of species with proper properties. In this thesis the cohesive aspect of particle is highlighted. Based on the reviewed literature a potential derived cohesive force is implemented, due to its clear geometrical representation of the force field, and its relative ease of implementation. It expresses firstly as a potential:

$$U_{morse} = D_e \left[1 - e^{\beta(r-d))}\right]^2$$

which is inspired from the article of [Yazdani et al., 2017] that preferred it due to its soft core compared to other potentials, allowing a smooth handling of particle repulsion used to avoid contacts. The associated force is obtained derived by derivation:

$$F_{cohes} = -\frac{\partial U_{morse}}{\partial r} = 2D_e\beta \left[e^{-2\beta d(r/d-1)} - e^{-\beta d(r/d-1)}\right].$$

$d[m]$ is the particle diameter and $\beta[m^{-1}]$ can be seen as a geometrical tuning parameter for the shape of the force function. $D_e[Nm]$ is a dimensional parameter that has been determined experimentally. Maximum F_{cohes} corresponding to $(r/d)_{max}$ is given by $\beta D_e/2$. Figure 3.1 depicts the adimensional cohesive force as function of the adimensional distance from particle center. One sees that the cohesive force has practically no impact for $r/D \geq 3$, and that βd product modifies the influence of the long distance force. Choice for βd is set to 2.5 to promote near particle surface attraction.

Figure 3.2 illustrates particle configuration when inter-center distance r' corresponds to maximum force. When particles collide, the cohesive force is null. When particle tends to separate due to external interaction, the cohesive force increases with distance up to maximum force, then decreases rapidly with distance to almost vanish when r' is greater than threefold the particle diameter.

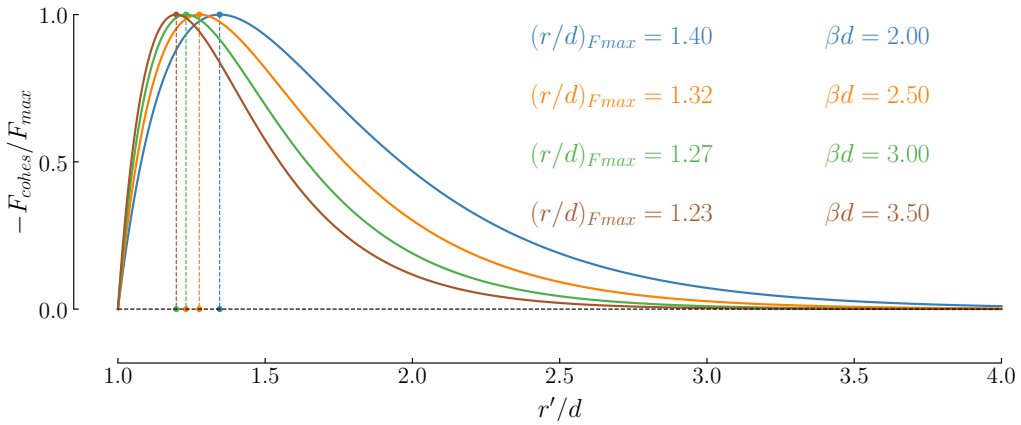

Figure 3.1: Impact of the product βd of the distribution of the adimensional cohesive force as function of the adimensional distance between two particles centers r'.

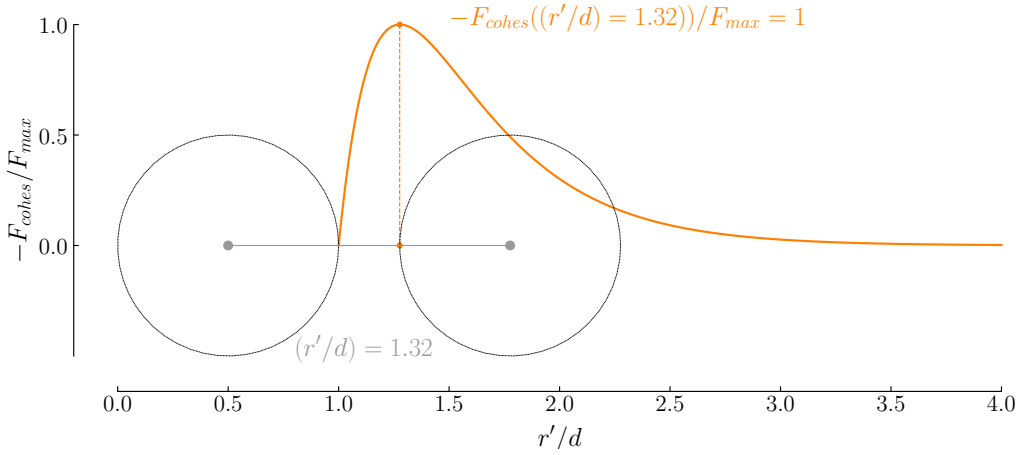

Figure 3.2: Corresponding particle spatial configuration at maximal cohesive force, for $\beta d = 2.5$

Numerical experiments consist first in a reproduction of a damaged channel subjected to a continuous flow of platelets. Simulations aim to observe phenomenological thrombus formation due to the introduction of a cohesive force intervening within the platelets population. The scale of the problem is then reduced according to real platelet size. The boundary conditions of the problem are depicted in Figure 3.3 and Table 3.1. Platelets are assumed to be activated along the domain. The injured endothelial is represented with help of a thin layer of cohesive fixed particles, providing an heterogeneous support for platelet cohesion. This layer is seen as an early deposit of platelets that have already aggregated at the site of injury. The flow is driven by an imposed Poiseuille profile, and the platelets inlet distribution is firstly considered as uniform.

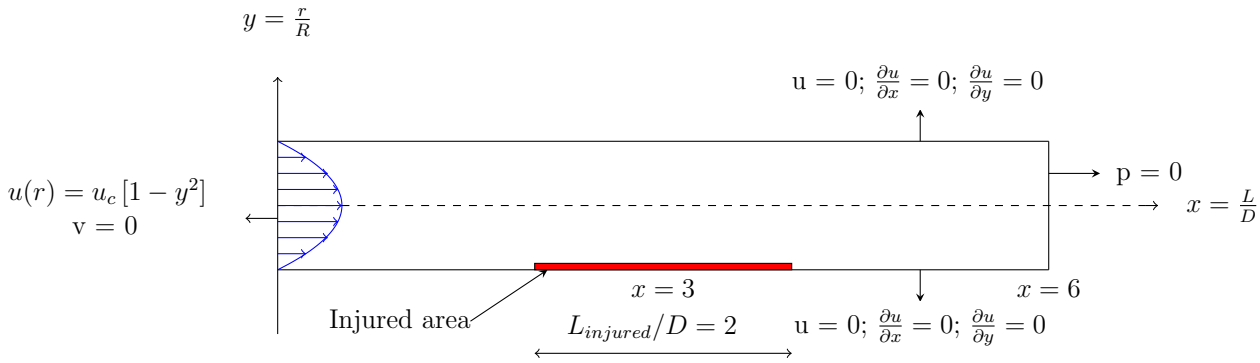

Figure 3.3: Thrombosis : problem conditions

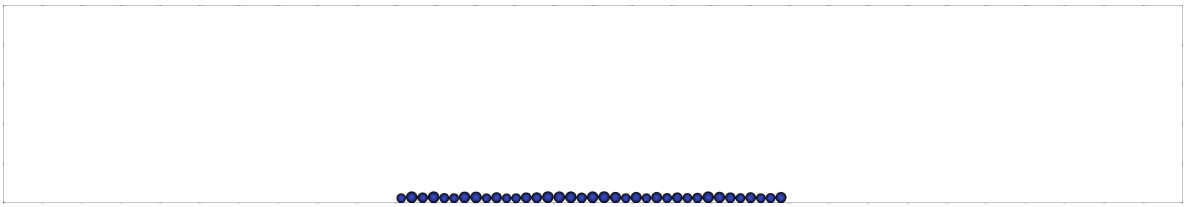

Figure 3.4: Initial domain configuration, with fixed grain population simulating the damaged vessel wall

Only the granular part of the suspension is considered in the first instance. It provides a more flexible background for simulation with only pure DEM. The cohesion calibration parameter D_e is firstly determined empirically to emphasize cohesion impact within particle population, and provide to illustrative results. A subtle decomposition of the suspension speed is however used to account for a virtual fluid drag:

$$\begin{aligned} \mathbf{u}_{susp} &= \mathbf{u}_{solid} + \mathbf{u}_{fluid} \\ \iff \mathbf{u}_{solid} - \mathbf{u}_{fluid} &= 2 \cdot \mathbf{u}_{solid} - \mathbf{u}_{susp} \\ &= \mathbf{v}_{rel}, \end{aligned}$$

where $\mathbf{u}_{susp}$ is the inlet imposed velocity profile.

The MigFlow softare is already implemented with a validated drag expression that characterises the fluid drag at each point *location* as a function of the *local* porosity $\phi|_{\mathbf{x}_i}$. In this case however such a local description of porosity is not available thus averaged to its mean over the simulation domain. An implemented function computes an image of the fluid drag at each time step over each particle considered as cylindrical with unit depth, given its speed, position and Reynolds number. The definition of the relative velocity v_{rel} allows to re-express the drag force:

$$\mathbf{F}_{drag} = \gamma\,(\mathbf{u}_{solid} - \mathbf{u}_{fluid}) = \gamma \mathbf{v}_{rel}$$

$$\gamma = \phi^{-1.8} \left(0.63 + 4.8/\sqrt{\frac{\sqrt{2}d\phi}{\mu}} \right)^2 d\frac{\rho_f}{2} \|\mathbf{v}_{rel}\|,$$

the blue term being the Reynolds number and ϕ being deduced from the number of platelets present within the domain Ω: $\phi = 1 - \frac{V_{plat}^{tot}}{V_\Omega}$. Despite impacting the method accuracy, it provides very representative results for the cohesive aspect of platelets interactions. First simulations results are presented in Figure 3.5 with $D_e = 1{\cdot}10^{-14}[Nm]$, simulation parameters are depicted in Table 3.1. Speed filters are all scaled according to the maximal speed of the imposed velocity profile $u_c = 2\bar{u}$. Results show the impact of an ambitious calibration of the cohesive law: grains interact rapidly and form branched structures. Those structures interact to form an heterogeneous thrombus network at the site of injury. Vessel obstruction is rapidly achieved, with progressive thrombus extrusion as more platelets are being injected.

	Variable		**Units**	**Values**
Geometrical parameters	Grain diameter	r_g	$[\mu m]$	1.5
	Domain height	D	$[\mu m]$	50
	Domain length	L	$[\mu m]$	300
Physical parameters	Grain density	ρ_g	$[kg/m^3]$	1050
	Mean speed	$\bar{u}$	[m/s]	$1{\cdot}10^{-3}$
Numerical parameter	discretisation step	Δt	[s]	$5{\cdot}10^{-5}$

Table 3.1: Trombosis: DEM simulation parameters

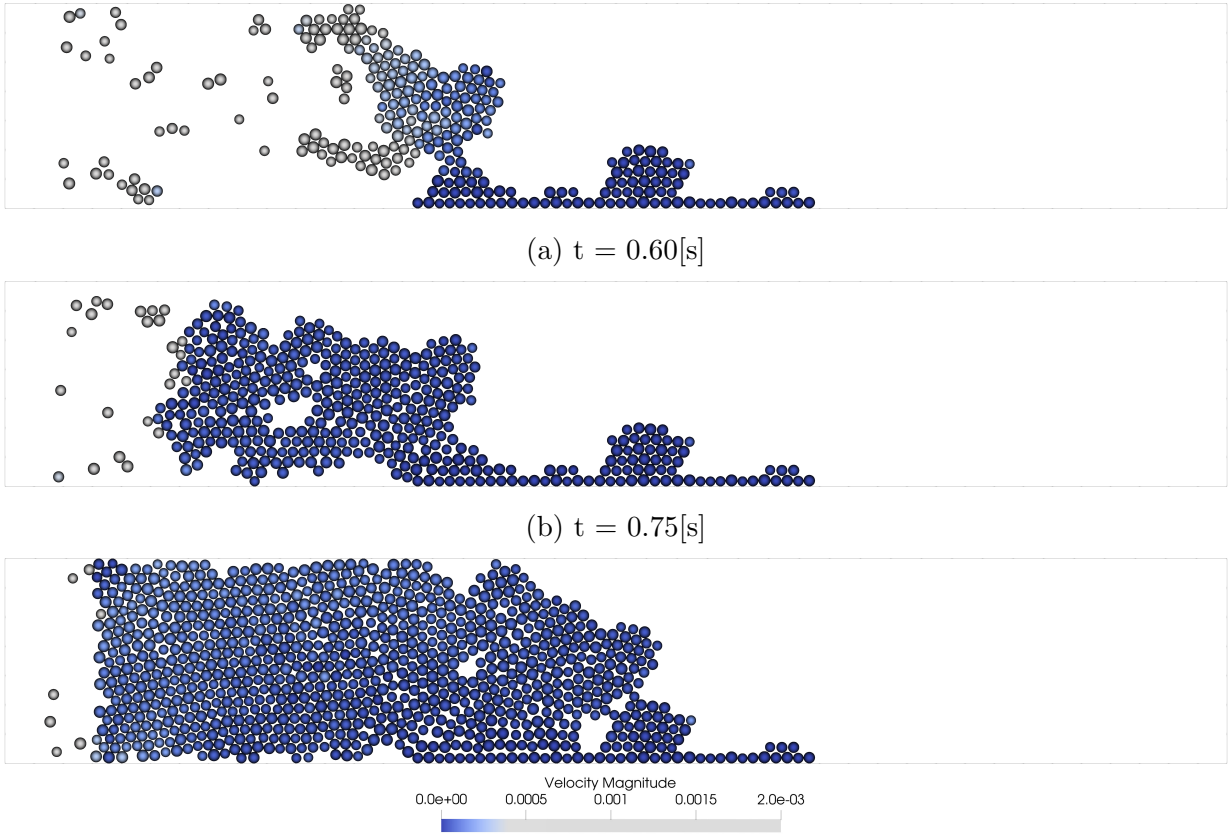

(a) t = 0.60[s]

(b) t = 0.75[s]

(c) t = 1.27[s]

Figure 3.5: Cohesive particle population under strong cohesive law parametrisation. In (a) and (b) particles interact forming branched structures, with network-like thrombus. Calibration lead to vessel obstruction and slow extrusion of the thrombus. Strong speed coloration filter is applied on particles to explicitly show immobilized particles

This configuration is far from being an accurate representation and motivates an empirical modification of the intensity of the cohesive law through adjusting parameter D_e by dividing it by 20. Observed platelets aggregates leaving the domain should desegregate downstream since we only consider activated platelets over the domain on which they exhibit cohesive properties. A softer calibration of the cohesive force (Figure 3.6) can provide more appropriate results: progressive and non obstructive thrombus build up is achieved. The more thrombus volume grows the more platelet interacts, forming platelet aggregates leaving the site of injury.

However, one should acknowledge that there is a trade-off between the amount of injected platelets, and the intensity of the cohesive force. If the force is too large, rapid obstruction occurs, and does not allow the platelets to interact and cover the injury site. At the opposite, weak forces does not not allow platelets to lose enough momentum to immobilize at the injured area and start to interact with other moving particles.

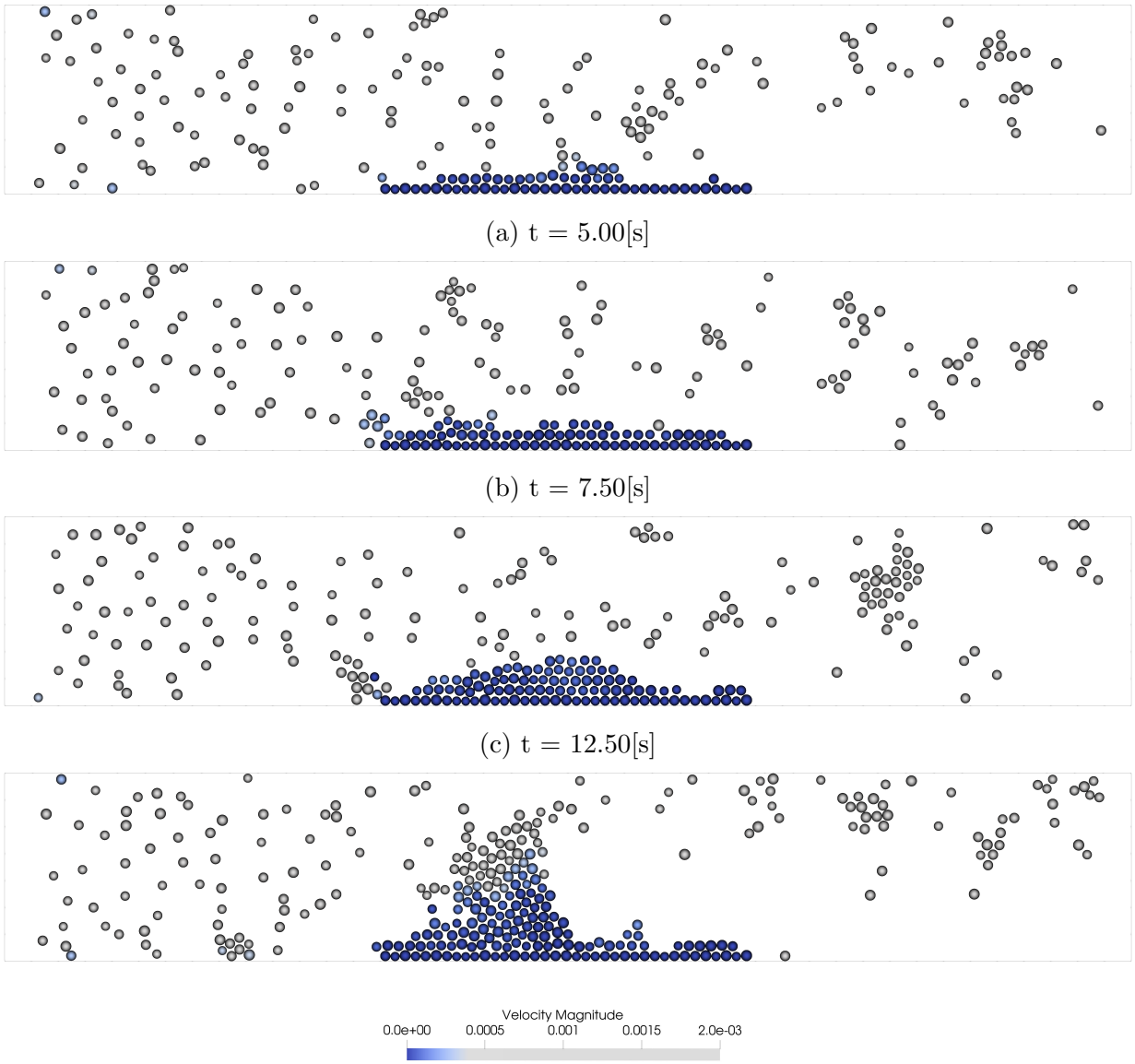

(a) t = 5.00[s]

(b) t = 7.50[s]

(c) t = 12.50[s]

(d) t = 15.15[s]

Figure 3.6: Cohesive particle population under smoothed cohesive law parametrisation. (a) shows thrombus initiation with first aggregation of particles. Platelet aggregation continues in (b) and (c). (d) shows thrombus destabilisation. Speed coloration filter is applied on particles to explicitly show immobilized particles

Since no fluid is yet taken into account, a sufficient number of platelets needs to be inserted to represent the flow tendency. If overall platelets compacity is too large, strong interaction occurs, and platelets rapidly bound by cohesion. Controversly, an sufficient number of platelets is necessary such that platelet inertia can unbound particles aggregates.

3.4.1 Platelets margination

It has already been established that blood hemodynamics is mainly influenced by the predominance of red blood cells. The deformable RBCs are known to induce near wall excess of platelets due to their migration towards the center of the flow. This leaves a gap in the near-wall region, where platelets concentration is increased. This naturally allows platelets to be already concentrated at the wall, where they are of primary importance for coagulation in case of vessel lesion or injury. This phenomenon is known as the Fåhræus effect [Fåhraeus, 1929] while the Fåhræus-Lindqvist effect [Fåhræus and Lindqvist, 1931], describes the local decrease of apparent viscosity due to RBC migration toward flow center and platelet excess in the near-wall region. That effect is more consequent with decreasing vessel diameter, reducing flow resistance in small arteries and capillaries. [Eckstein et al., 1988] describe the effect of vessel radius and wall shear stress on near wall platelet excess distribution. [Leiderman and Fogelson, 2011] take account of a near-wall excess of platelet concentration in their model with an imposed platelet concentration profile. In this case study, platelets margination is modeled in a similar way with help of a beta distribution over the insertion height at the vessel inlet as depicted in Figure 3.7.

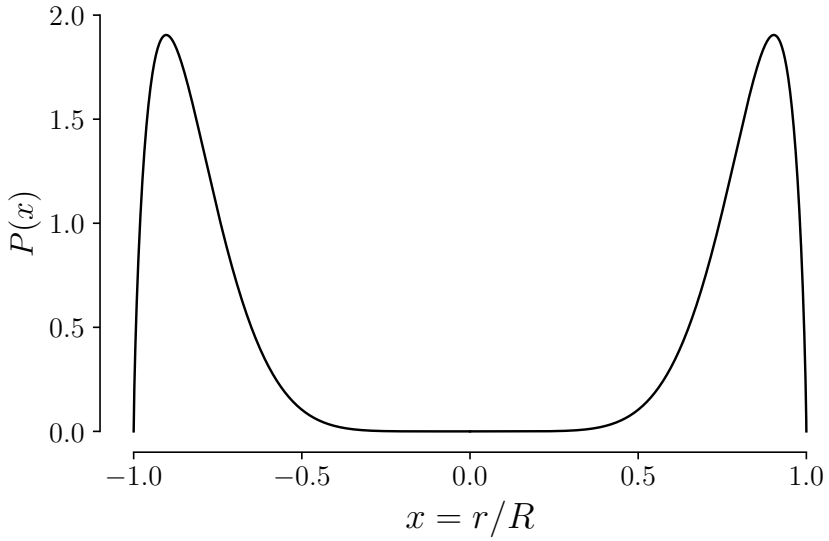

Figure 3.7: Probability density function of the platelet inlet distribution profile as function of adimensional radial position, built from beta distribution $\sim \mathcal{B}(8, 1.75)$.

Trade off emerges again from parametric studies on cohesion intensity and platelets number. Firstly, thrombus growth begins at the most upstream region of the site of injury. Following near wall platelets bounce on this first obstacle, and interact with other platelets forming aggregates that push the obstacle, thus enlarging the thrombus over the injury length. If platelet compacity is increased, stronger mid-height particle aggregates form and constantly interact with the forming thrombus. In the contrary, platelet rarefaction increases growth rate and favors obstruction with weaker interactions. Due to those observed aspects, platelet margination is rather used with presence of RBCs considered as an external non

cohesive particle population.

3.4.2 Impact of additional non cohesive specie

The thrombus formation is numerically investigated with an additional specie: the red blood cells. Since their deformability properties are not considered in this work, they are represented by spherical particles. The size ratio between RBCs and platelets is nevertheless respected and RBCs are assumed to be normally distributed over 50% of the vessel diameter to simulate their migration towards flow center. They have similar density compared to platelets ($\rho_{rbc} = 1110[kg/m^3]$) and are modelled as platelets with a size ratio comparable to maximum diameter ratio observable in reality : $r_{RBC} = 8/3 \cdot r_p$. Results are shown in Figure 3.8, the cohesive parametrisation is kept constant as in Figure 3.6.

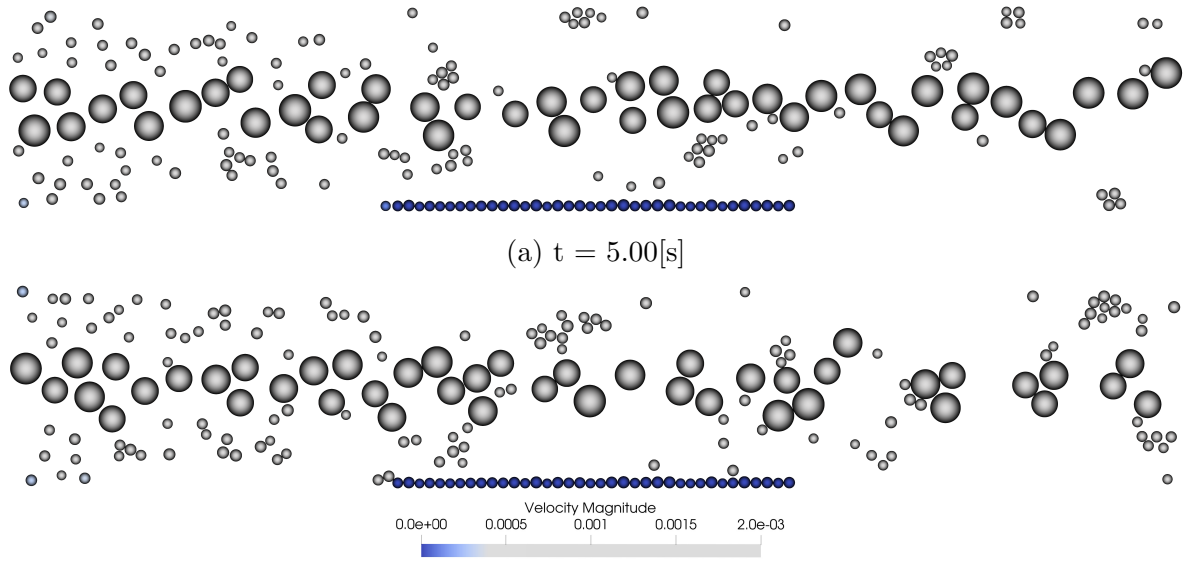

(a) t = 5.00[s]

(b) t = 10s[s]

Figure 3.8: Impact of external non-cohesive greater particle specie on cohesive population of platelets. Cohesive forces are too weak to allow aggregations.

There is a strong impact of non cohesive RBCs on platelet aggregation tendencies. Platelets form aggregates in marginalised region, but cannot form stable clot at the injury site due to their interaction with RBCs. This motivates a new empirical calibration of the cohesive law. Figure 3.9 presents the same numerical experiment with doubled cohesive force intensity. Platelets do now aggregate at the site of injury, the cohesive force being sufficient enough to allow interactions. Aggregates form and encounter other aggregates that have already bounded with the injury. The resulting congestion promotes interactions of a large number of platelets which is then flattened over the injury by the flow of RBCs. One observes that RBCs have a regulatory role in thrombus formation by containing platelets near the vessel wall. Presence of additional cell population inhibits the formation of big platelets aggregates at flow mid-height that could lead to occlusive events. Coagulation is then favored at the injury site with constant platelets interactions. However, no permanent

thrombus is observed. One understands the importance of both calibration and flow inertia in thrombus formation. With pure DEM approach, one has put forward the sensitivity of the calibration and the importance of the flow description.

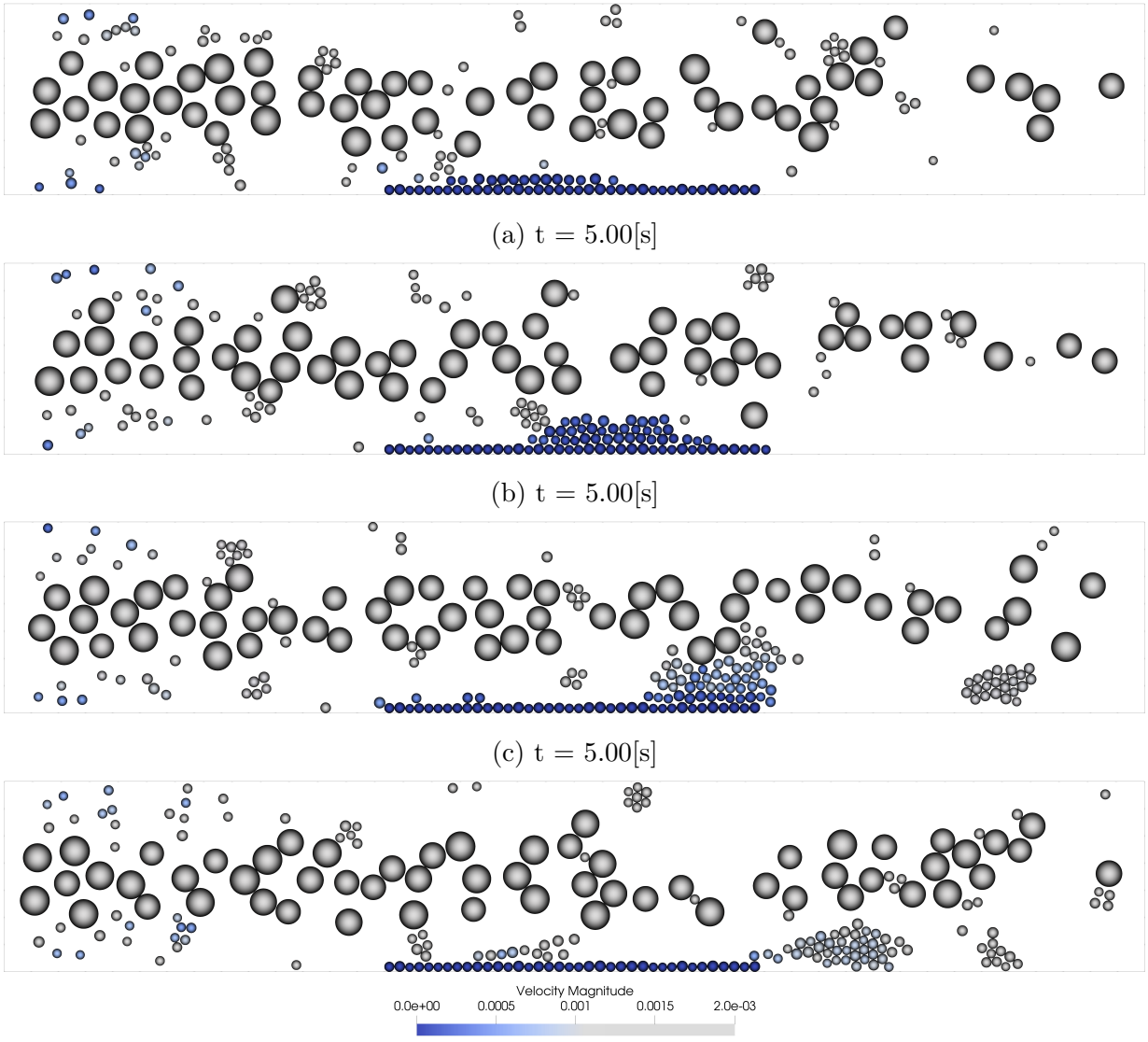

(a) t = 5.00[s]

(b) t = 5.00[s]

(c) t = 5.00[s]

(d) t = 10s[s]

Figure 3.9: Impact of external non-cohesive greater RBCs particles on cohesive population of platelets with doubled cohesive force intensity. (a) and (b) show platelet deposits at the site of injury. (c) and (d) show interaction between aggregated platelets at the injury and RBCs that further destibilizes the clot and push it downstream of the injury site

3.4.3 Impact of the fluid

Pure DEM approach is now coupled with a precise fluid description. Grains parameters are kept constant and the cohesion intensity is set back to the smooth calibration illustrated in 3.9. Simulation mesh is provided in Figure 3.10. Fluid is modelled with respect to averaged

plasma properties: $\rho_f = 1025[kg/m^3]$, $\mu_f = 1.2 \cdot 10^{-3}[Pa \cdot s]$. Adimensionnal representation of the flow provides a Reynold number of ≈ 0.04 given the scale of the experiment.

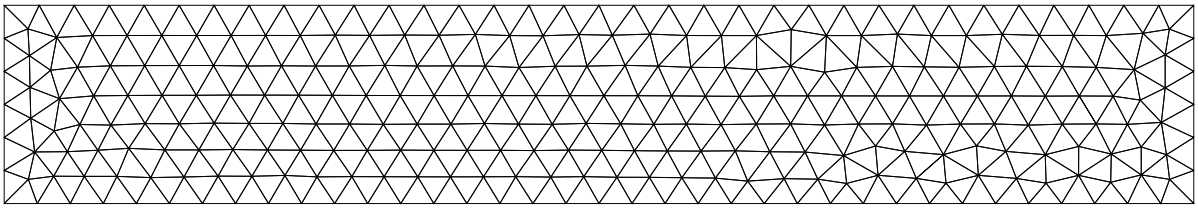

Figure 3.10: Fluid simulations mesh.

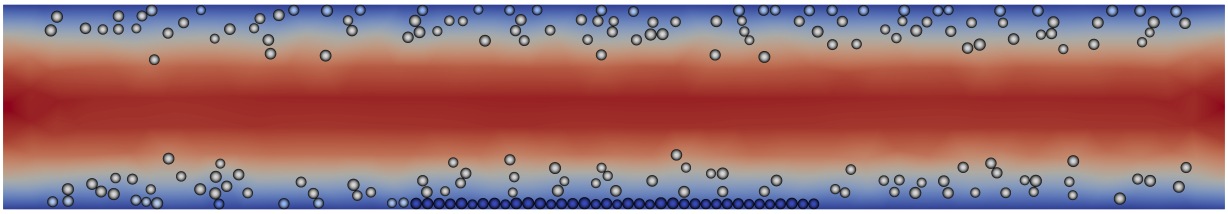

(a) t = 5[s]

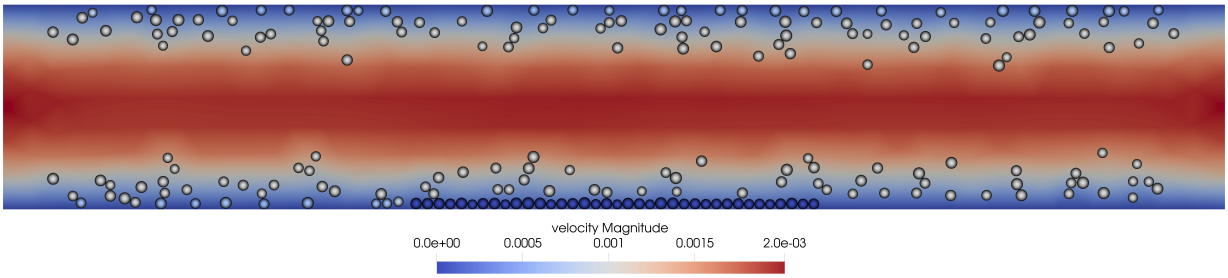

(b) t = 10[s]

Figure 3.11: Simulation results of a cohesive platelet population coupled with an enhanced fluid representation.

Simulation results in Figure 3.11 show that the fluid phase is a game changer with regard to cohesion and considerably enhances the description of the particles behaviour within the suspension in the same time. It is considerably impacting observations of pure DEM experiment with same parameters. This is however not surprising regarding the impact of the inertia of an auxiliary population. Fluid has comparable effect to RBCs, but with far more precise description. A new empirical calibration of the cohesive force brings results closer to the pure DEM approach as observed in Figure 3.12, with $D_e = 1.5 \cdot 10^{-11}[Nm]$. However, those results are less demonstrative and constraint the method due to the stiffer response of the cohesion. Platelet accumulation is observed, but large thrombus formation is not observed. It is difficult to provide an exhaustive description of the cohesive law with realistic parameters regarding the explicited underlying bio-chemical processes. Their description and calibration are not the objectives of this work. Physiological cohesive effects are reproduced but, individually speaking, the cohesive aspect of activated platelets is insufficient to provide an accurate representation of the thrombus formation mechanism.

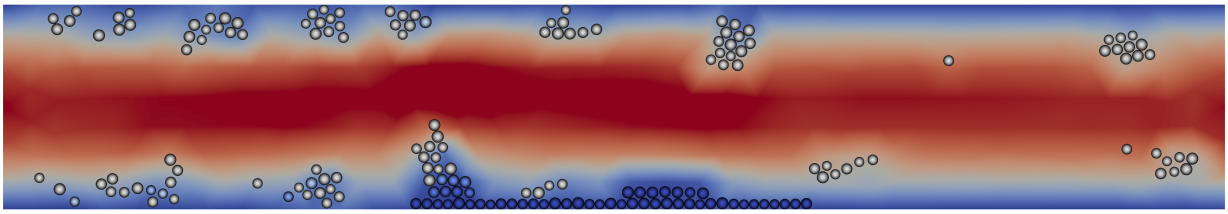

(a) t = 0.25[s]

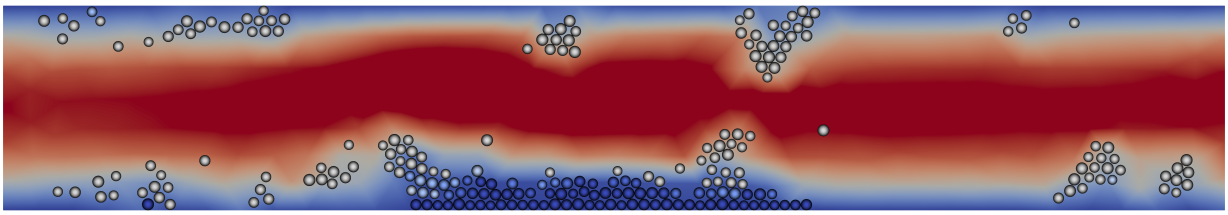

(b) t = 0.75[s]

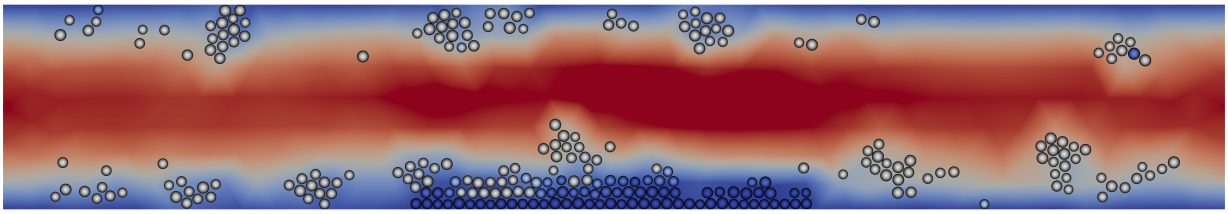

(c) t = 1.00[s]

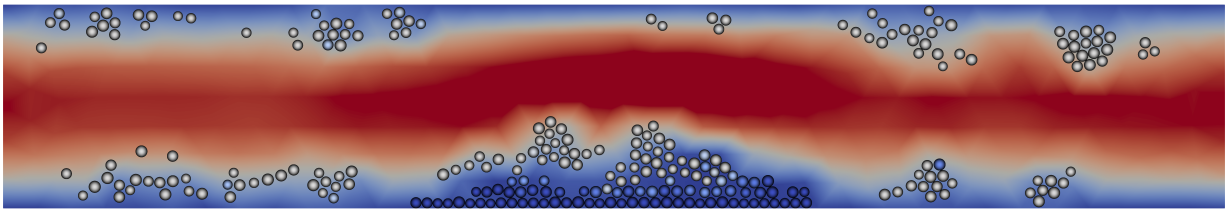

(d) t = 1.50[s]

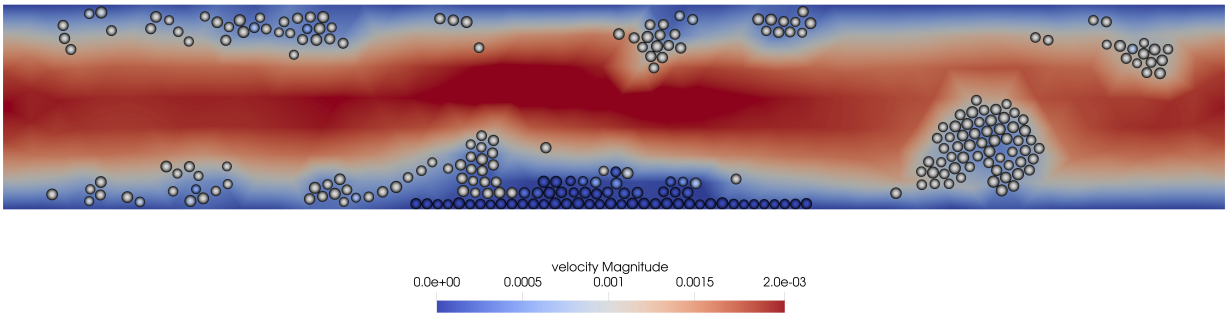

(e) t = 3.45[s]

Figure 3.12: Aggregating platelets behaviour for enhanced Morse law calibration. Speed filter is applied to particles to show immobilisation (in blue). (a) and (b) show progressive deposition and aggregation of platelets on the injured area. (c) and (d) show platelets detachment resulting from platelets interactions. (e) shows rupture of the covering plaque with large aggregates leaving the injured area

3.5 Outcomes

This chapter depicts the biological landscape of thrombus formation. A review of the existing methods within the literature shows the advantage of the approach presented in this master thesis. The fluid-particle coupling allows at first to include a precise cellular description within the granular flow compared to contiuous models, and also take advantage of the concrete contact resolution with the NSCD method. Moreover, this chapter reflects the validation of the implementation of the cohesive force within the method from a numerical point of view. It robustness is also demonstrated with a stiffer calibration of the cohesion.

Chapter 4
Stenosis

4.1 Context

Atherosclerosis is an arterial narrowing progressive disease characterised by a local formation of atheroma plaques within the artery wall. This geometrical modification of the arterial tunic is due to the accumulation of lipids, inflammatory cells, extracellular matrices, originating from an excessive presence of cholesterol. The evolution of the plaques takes place over a long period of time, from several years to multiple decades. When the plaque deposit becomes too large it can dangerously reduce the lumen cross section area and eventually provoke ischaemia (restriction of blood to tissues, or organs). The resulting atherosclerotic plaque can later evolve to form a stenosis and can alter the hemodynamics of the blood flow along the artery.

Artherosclerotic characterisation is quite new regarding history. Its first comprehensive approach dates form the 19^{th}. century. In 1856 Rudolph Virchowl [Virchow, 1856] proposed a correct theory on the pathogenesis of the atherosclerosis, stating that atherosclerosis was the combination of an inflammatory and proliferating process within the intima. The contemporary understanding of the disease is based on the work provided by [Ross et al., 1977] later improved in [Ross, 1999], who completed this hypothesis by adding the intimal accumulation ans proliferation of smooth muscle cells. The conclusions established by Ross are the basis of today's comprehension of the disease proposing that atherosclerosis lesions are the result of a local endothelial damage followed a.o. adherence, aggreation and release of platelets.

Cholesterol excess has been proven [Anitschkow and Chalatow, 1913] to be the principal element factor leading to atheroma plaque formation and is consequently responsible for the initiation of atherosclerosis. Lipoproteins are the main transporters for lipids such as cholesterol. Produced in the liver, they are transported by blood plasma toward tissues and cells to provide lipids (cholesterol) for cellular metabolism.

One should distinguish two types of lipoproteins:

- Low density lipoprotein (LDL): Ensures transport of hydrophobic fatty contents such as cholesterol, triglycerids into a cap of hydrophillic proteins from secretion points to the organism cells where cholesterol is needed for membrane reparation.
- High density lipoprotein (HDL): Secreted in the liver, it ensures the discharge of excess cholesterol among the organism and its degradation or redistribution back into the liver. Interesting to note is that woman are more prone to HDL production due to enhanced oestrogene production and are therefore less exposed to atherosclerosis.

At atherosclerosis initiation, the LDL transporting cholesterol passively diffuses throughout the endothelium. There, the LDL molecule undergoes oxidation within the intima in

presence of free radicals such as oxygen radicals forming ox-LDL molecules.

The ox-LDL lipoproteins have a specific affinity response with the scavenger receptors of the macrophages (white blood cell) migrating from the plasma to the artery wall. This promotes the formation of foam cells by internalisation of ox-LDL. Those foam cell liberate immunological stimulant citokines which trigger an inflammatory process within the arterial wall. This tends to increase the permeability of the endothelium and consequently amplifiy the inflammation. The local accumulation and colonisation of the intima by these macrophagous spumous cells constitutes the first response: the *fatty streak*.

Liberated Citokins also initiate the migration of the smooth muscular cells (SMC) from the media to the intima. Those cells start to secrete a complex extracellular matrix containing collagen, forming the *fibrous cap* covering the fatty streak. SMC migration and proliferation is usually contained under normal endothelial behaviour through endothelial production and release of nitric oxyde. This lipidic aggregation forms the so called *atheromous plaque*, setting the pathological basis for the atherosclerosis.

The evolution of the geometry and volume of the plaque is balanced by cellular apoptosis, cellular necrosis and SMC migration. The growth mechanism involves diverse quantities of species but can be here simplified. Spumous cell necrosis or apoptosis favour the attraction of macrophagous cells which interact to create extracellular lipidic deposits at the core of the atheromous plaque. Since this released content increases macrophage concentration, more ox-LDL are attracted within the intima and thus enhancing spumous cells creation, thus deepen the inflammation, and raise citokin concentration which in turn increases the migration of SMC and collagen production.

As the plaques start to grow, only wall thickening occurs without any lumen narrowing. The lipidic aggregate or atheromous plaque produce enzyme which cause the artery to enlarge over time. As long as the artery enlarges sufficiently to compensate for the wall thickening and extra thickness of the atheroma, then no narrowing of the lumen occurs.

At this point, rupture of the plaque can occur by ulceration or by plaque calcification. The release of the intra-plaque lipidic content triggers a coagulation cascade reaction. The coagulation process may form a thrombus which can obstruct the vessel as seen in previous section. During the hemostasis following the plaque rupture, a new fibrous cap covers the plaque lesion an can promote its growth and lead to the formation of a stenosis. Stenosis growth is then also due to *repetitive* plaque rupture and thrombosis formation initiated by coagulation. Thrombus are hazardous and are the primary cause of acute coronary events: lumen obstruction can occurs in case of fibrinolysis defects, inducing ischemia. Naturally, plaque rupture occasioned by thrombus defects (embolus) can obstruct small downstream vessels, leading to stroke or ischemia.

Stenosis volume increase directly affects the blood hemodynamics at the wall-blood interface and add an auxiliary contribution to the plaque desintegration due to the wall shear stress. Wall shear stress distribution will also locally enhance endothelial permeability to

lipoproteins or favor homeostasis molecules agglomeration near flow re-attachment. From a more global perspective, stenosis impacts the flow and provokes irreversible head losses, that can alter the irrigation of downstreams organs.

One understands the complexity of the intrinsic bio-chemical processes leading to plaque formation. Due to the central role of platelet observed in previous section, one study their behaviour in the context of atherosclerosis when exposed to cohesive environment.

4.2 Numerical Results

This section aims to study blood behaviour in the context of atherosclerosis. This thesis constitute a first approach to the understanding of atherosclerosis, and the platelets aggregation patterns are investigated. The following study is being developed around the area reduction or *stenose* being the principal physical manifestation of the disease, and its impact on blood naively modeled as a granular suspension of platelets.

4.2.1 Fluid approach

One studies first of all the fluid alone, with Poiseuille inlet speed distribution profile, through a stenosed canal. Stenosis is often described with an area reduction factor noted f_0. The effect of area reduction on the wall shear stress is investigated, as well as the size of the recirculation region. To this use, we consider a symmetric stenose whose geometry is imposed as:

$$h(x) = \pm R\left[1 - f_0\left(1 + \cos\left(\frac{2\pi(x - x_0)}{L_s}\right)\right)\right],$$

where L_s and x_0 designates respectively the stenosis length and center-edge. The boundary conditions and parameters of numerical simulations are observable in Figure 4.1 and Table 4.1.

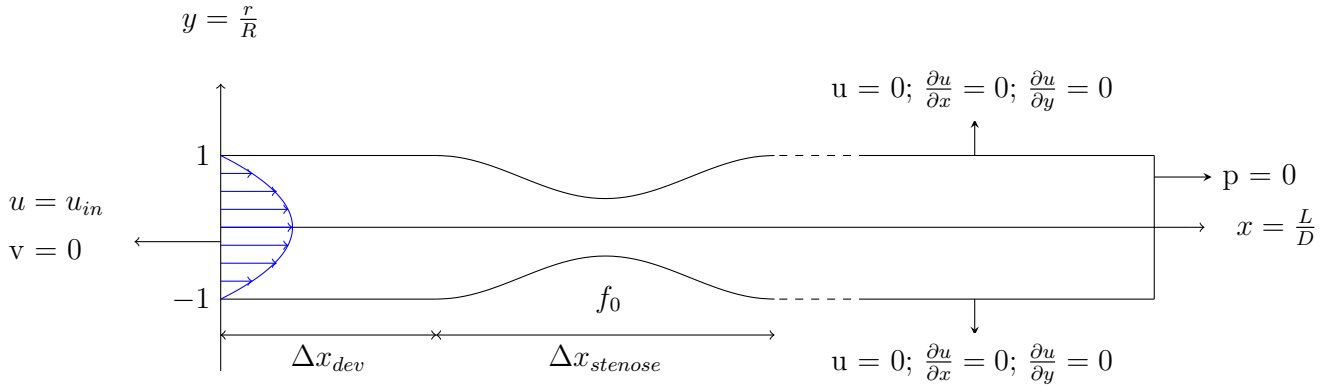

Figure 4.1: Stenosis: problem conditions

Where u_{in} is defined as:

$$u_{in} = u(y) = u_c \cdot \left(1 - y^2\right) = 2 \cdot \bar{u}\left(1 - y^2\right)$$

	Variable		Units	Values
Geometrical parameters	Domain height	D	[mm]	4
	Domain length	L	[mm]	80
	Area reduction	f_0	[-]	0.5 - 0.7
Physical parameters	Fluid density	ρ_f	$[kg/m^3]$	1060
	Fluid dynamic viscosity	μ	$[Pa \cdot s]$	$1.2{\cdot}10^{-3}$
	Reynolds number	Re	$[-]$	100 - 500

Table 4.1: Numerical values for fluid simulations.

The problem has been calibrated to reproduce the plasma conditions within a coronary artery. Given the huge variety of artery diameters and flow regime, the diameter is set to an intermediate diameter and low Reynolds number is assumed to approach real flow conditions at some locations within the circulatory system, i.e. carotid artery. Figures 4.3 to 4.5 show impact of Reynolds number ($Re = 100, 300, 500$) and area reduction ($f_0 = 0.5, 0.6, 0.75$) on the flow in the post stenotic region.

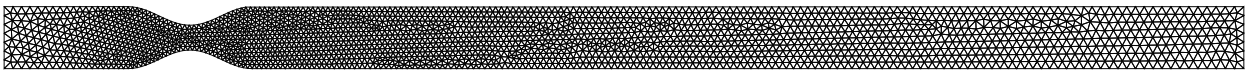

Figure 4.2: Stenosis mesh for fluid analysis, aspect ratio L/D = 20, $\Delta x_{dév} = \Delta x_{stenose} = 2$

(a) Re = 100

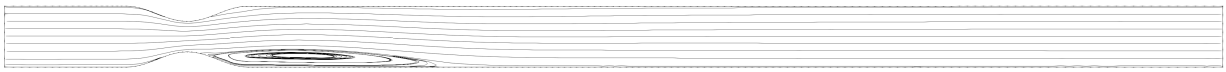

(b) Re = 300

(c) Re = 500

Figure 4.3: Impact of Reynolds number for 50% area reduction, t = 10[s]

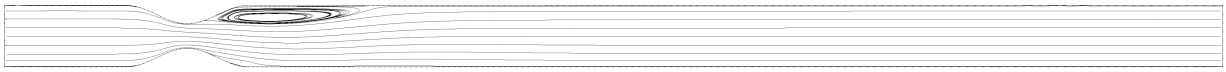

(a) Re = 100

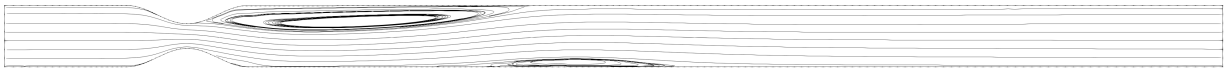

(b) Re = 300

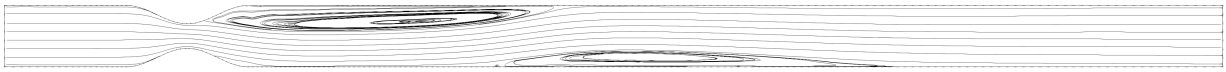

(c) Re = 500

Figure 4.4: Impact of Reynolds number for 60% area reduction, t = 10[s]

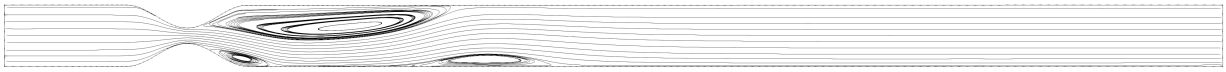

(a) Re = 100

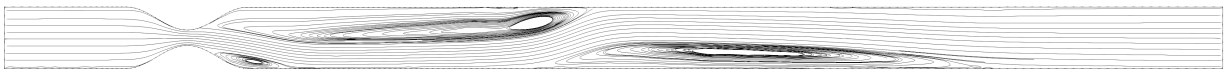

(b) Re = 300

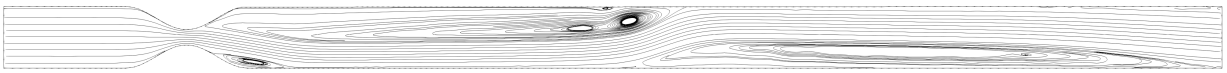

(c) Re = 500

Figure 4.5: Impact of Reynolds number for 75% area reduction. t = 10[s]

The choice of flow regime studied in this thesis ensures a laminar flow in the whole domain without transition to turbulence. [Varghese et al., 2007] predicts a laminar post-stenotic region for inlet Reynolds lower than 1000. As stenosis changes the velocity distribution, Figure 4.3 to 4.5 clearly illustrate the tendency of the fluid to accelerate at the beginning of the stenosis as the flow area decreases. At the stenosis throat, the speed uptake can raise from three to nine times the mean imposed inlet velocity $\bar{u}$. Past the stenotic throat one observes flow detachment leading to re-circulation regions in the post-stenotic region. The increasing size of those recirculating zones are associated with the importance of the area reduction f_0 that provides steep positive pressure gradients.

A clinical quantity of interest is the force of the suspension on the vessel wall. Figure 4.6 shows the evolution of the wall shear stress of the fluid for increasing Reynolds. High shear stress at the stenosis throat may favour plaque rupture in one hand, but would reduce time of residence thus probability of diffusion and adhesion of blood cells such as macrophages or platelets within the atheromous plaque [Parmentier et al., 1977] on the other. Low shear stress regions in the contrary, predominent at the stenosis shoulder in the post stenosis region (re-circulation zone) favours platelets aggregation and plaque growth. Those protective and destructive effects of wall shear stress on the atheromous plaque and thrombus was highlighted by [Ku et al., 1985].

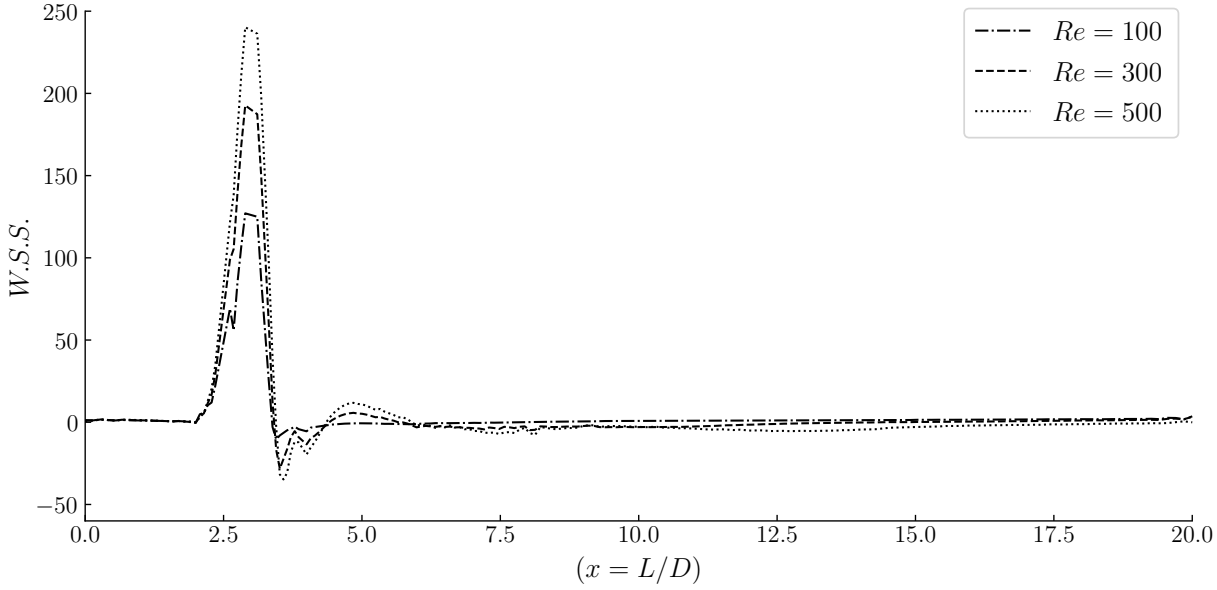

Figure 4.6: Wall shear Stress evolution with increasing Re, for fixed 60% area reduction. W.S.S is centered with respect to its mean value upstream of the stenosis

4.2.2 Granular steady flow approach

Flow behaviour is further investigated as platelets are introduced. One studies their behaviour and their trajectories across the liquid media. The numerical simulation first proceeds to a fluid stabilisation until steady flow conditions are reached, then grain insertion begins within a small column of the numerical domain, forming the suspension. Particles insertion is achieved within a small partition of the upstream domain. One or multiple grains is inserted at each time step. Positions of the particle population within the insertion zone are evaluated to place the future generations and avoid interpenetration. Similarly, particle positions are constantly monitored to remove them at the end of the vessel. Figure 4.7 shows the numerical mesh used for the simulations, attention being paid to set element size according to particle diameter. The chosen mean inlet speed $\bar{u}$ ensures Re = 100. Such laminar regime is more prone for particle monitoring.

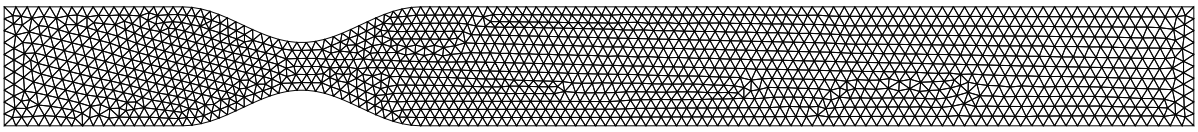

Figure 4.7: Stenosis mesh for granular simulations, aspect ratio L/D = 10

Figure 4.8 shows the suspension behaviour when a population of particles is subjected to a constant Poiseuille inlet flow, for $(f_0, Re) = (0.6, 100)$. Stationary fluid stabilisation is not waited before beginning particle insertion, but short fluid solution propagation is achieved preceding particle insertion. Under those conditions, particles are accelerated through the stenosis and are concentrated in a stream-*tube* past the stenosis throat. One observe however that the suspension tends to the same behaviour as the fluid solution: a preferential recirculating zone is "chosen" at the expense of the other, resulting in a symmetry loss despite laminar flow and low Reynolds number. This effect is linked to the two-dimensional numerical strategy. An axi-symmetric numerical framework would provide a better (symmetrical) description of the fluid, but is would complexify particles description. Particles slowly penetrate into re-circulation zones up to the stenosis wall, but this seems mostly due to fluid transient effects occurring downstream of the stenosis, whose amplitude scales up with time, rather than to a spontaneous response.

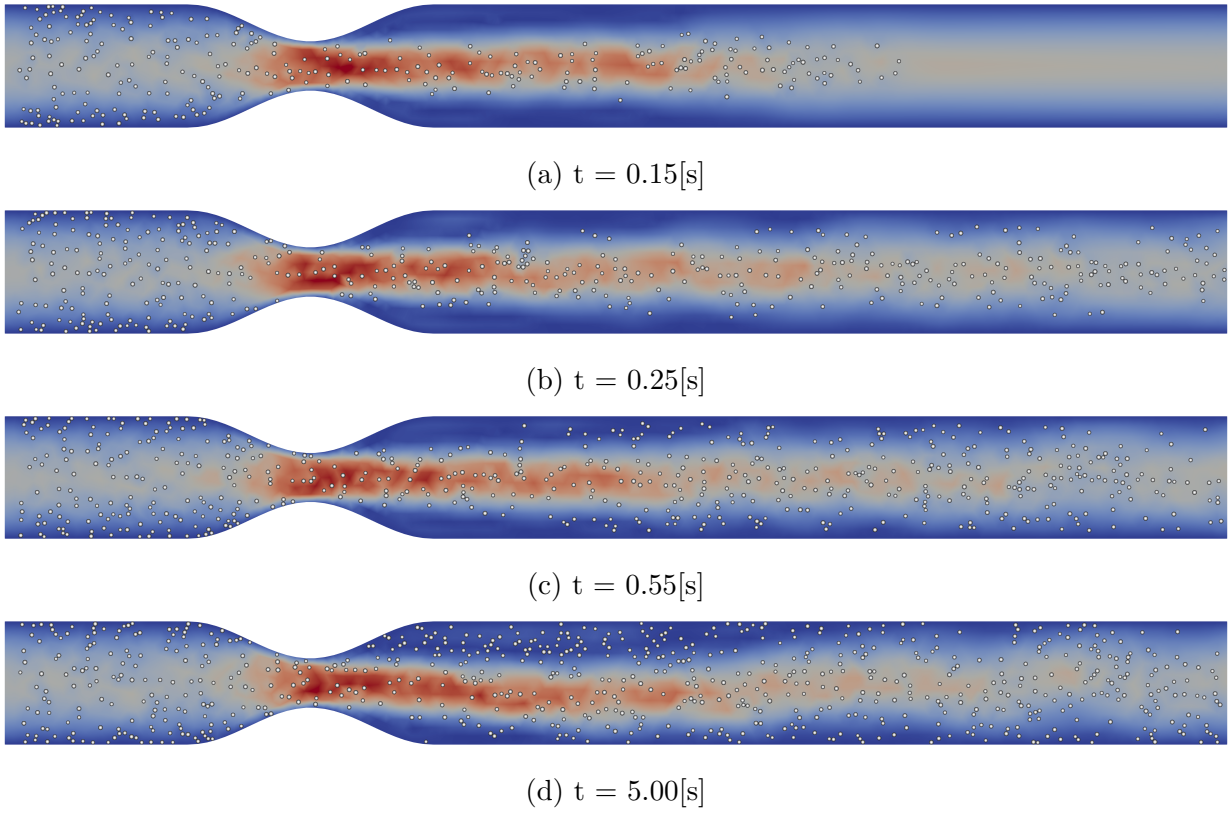

(a) t = 0.15[s]

(b) t = 0.25[s]

(c) t = 0.55[s]

(d) t = 5.00[s]

Figure 4.8: Platelet behaviour under Poiseuille flow with 60% stenosed canal. Temporal values are based on initial platelet insertion time and fluid viscosity aligned to that of the blood

As one would expect that at this stage of development platelets would already pack in the post stenotic region, one understands that a steady representation of the flow may not be very representative for platelets behaviour. Indeed, presence of platelet near the stenosis wall seems mostly due to downstream conditions which are idealised in this case (straight tube) and favour upstream platelet migration. These observations motivate the choice of the pulsatile approach.

4.2.3 Granular pulsatile flow approach

Pulsatile blood flow inlet conditions constitute an improvement of the simulation, bringing it a step closer to real conditions. Using the well known results developed by [Womersley, 1955]who proposed an exact analytical solution for fully developed laminar flow in rigid arteries under pulsatile conditions, the velocity profile imposed at the vessel inlet is yet defined by:

$$\frac{u}{\bar{u}} = \left[1 - y^2\right] + A\left[\frac{1 - J_0(i^{3/2}4yW_o)}{J_0(i^{3/2}\alpha)}\right]\cos(\omega t), \tag{4.1}$$

which translates into a superposition of the Poiseuille velocity profile with an oscillating component, where J_0 is the Bessel function of type 0, A is the amplitude of the pulsed component and W_o is the adimensional Womersley number. This number is defined as

$R\sqrt{\omega/\nu}$ with ω the angular frequency of the blood pulsation. It relates the importance of unsteady and viscous forces. Typical values of Womersley number range between 1 to 10 in arteries. $\bar{u}$ is now defined as the cycle average centerline speed, corresponding in this case to the maximal velocity u_c of the Poiseuille profile.

	Variable		**Units**	**Values**
Pulse parameters	Reynold Number	Re	$[-]$	200
	Pulse amplitude	A	$[-]$	0.667
	Pulse frequency	f	$[Hz]$	1.333
	Pulse angular frequency	ω	$[rad/s]$	0.298
	Womersley Number	Wo	$[-]$	3.185

Table 4.2: Pulse properties based on human artery size and averaged heart pulsation frequency.

The choice of pulsatile flow is motivated due to the introduction of suction phase, which is not described with a simple Poiseuille approach. This allows to describe more precisely the suspension dynamics and enhance the mixing of particle within the flow, as they get pulled back in the post stenotic region.

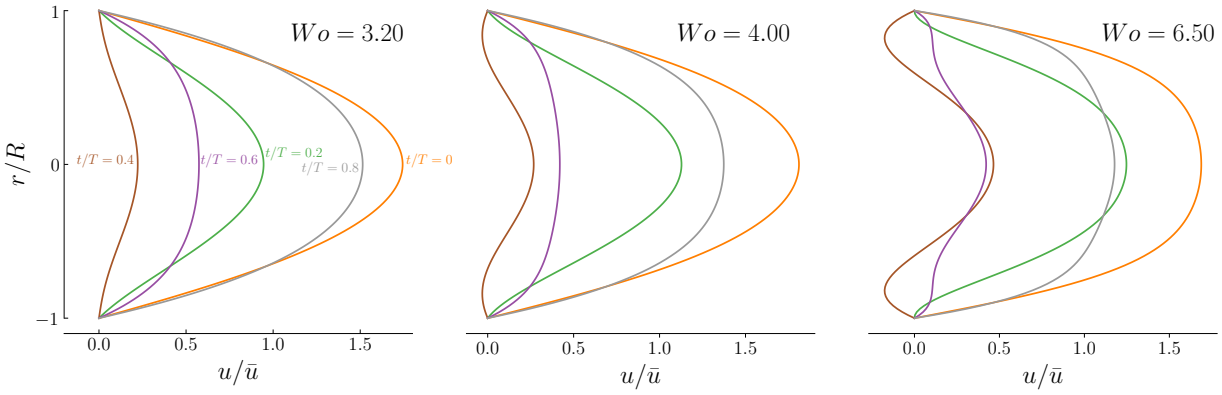

Figure 4.9: Adimensionalised inlet velocity profile as function of Womersley number Wo. Different curves correspond to equidistant period intervals, separated by $t/T = 1/5$

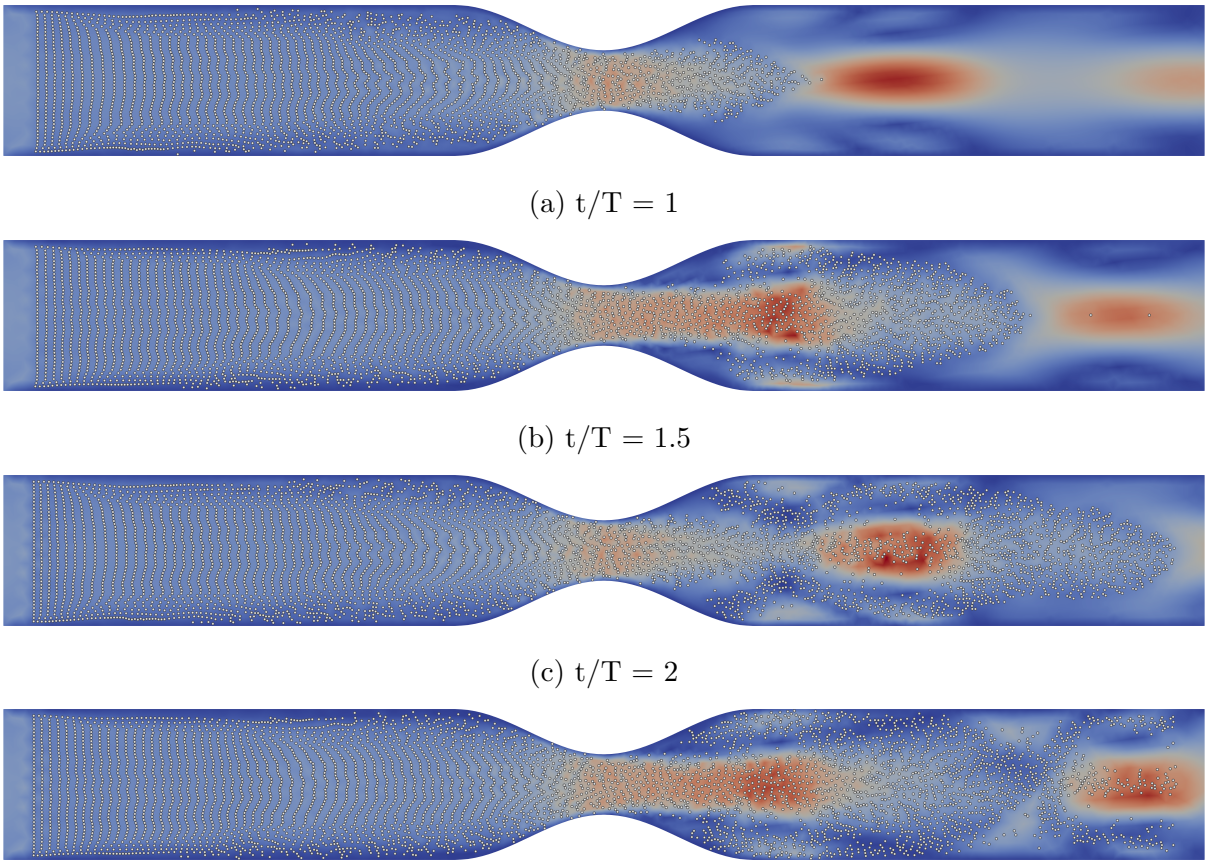

(a) t/T = 1

(b) t/T = 1.5

(c) t/T = 2

(d) t/T = 2.5

Figure 4.10: Explicit demonstration of enhanced grain behaviour trajectories past the stenosis throat. $Re \approx 200$, $Wo \approx 13$, $\rho_p = 3 \cdot \rho_f$, $\nu = 4.5 \cdot 10^{-3}[m^2/s]$

Figure 4.9 shows the adimensionalised velocity profile of equation 4.1 for different fractions of a time period and for increasing values of Womersely number. The importance of the conter-flow and the flatness of the profile at maximal amplitude increases with Womersley number. Those effects are observed in Figure 4.10, representing a very dense suspension with exaggerated flow properties for illustrative purpose. Figure 4.11 illustrates the behaviour of particles past the stenotic throat for this flow configuration. Clearly, particle circulation in the post stenotic zone near the stenosis wall is improved with pulsatile inlet conditions when compared with Poiseuille flow conditions.

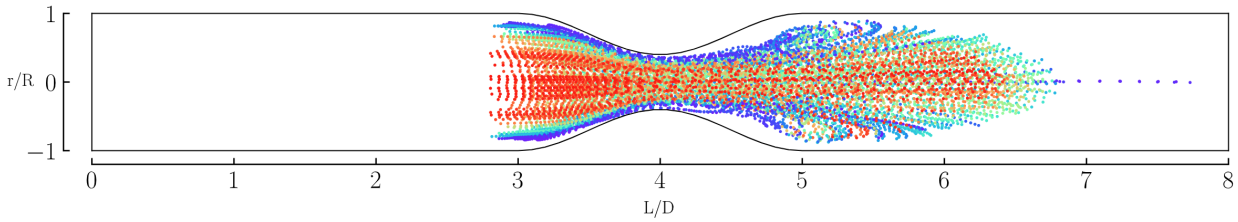

(a) Particles trajectories tracking for granular flow under pulsed conditions, grains being inserted at the vessel inlet. Each grain has associated color for identification visibility

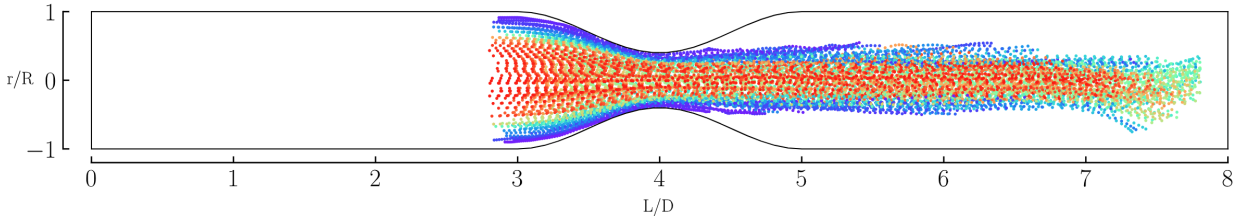

(b) Particles trajectories tracking for granular flow under Poiseuille conditions.

Figure 4.11: Comparison of particles trajectories given inlet conditions. Each grain has associated color for identification visibility

	Variable		**Units**	**Values**
Geometrical parameters	Grain diameter	r_g	[mm]	0.08
	Domain height	D	[mm]	2
	Domain length	L	[mm]	40
	Area reduction	f_0	[-]	60
Physical parameters	Fluid density	ρ_f	$[kg/m^3]$	1060
	Fluid dynamic viscosity	μ	$[Pa \cdot s]$	$3.5{\cdot}10^{-3}$
	Grain density	ρ_g	$[kg/m^3]$	1060
	Centerline av. mean speed	$\bar{u}$	$[m/s]$	0.33
Numerical parameters	discretisation step	Δt	[s]	$1{\cdot}10^{-4}$

Table 4.3: Simulation parameters for platelets simulation in stenosed artery

Following simulations are now based on more realistic blood parameters based on its averaged values at $37[^{\circ}C]$, as depicted in Table 4.3. Fluid behaviour under those parameters is investigated and results are presented in Figure 4.12, where clear re-circulating zone build-up is observed.

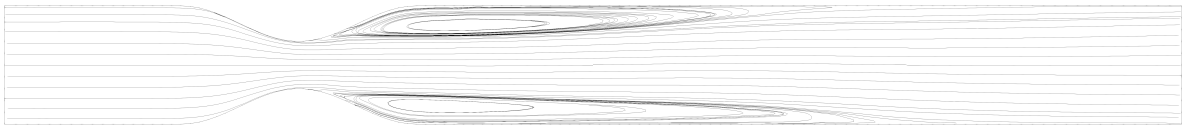

(a) t/T = 0.0

(b) t/T = 0.20

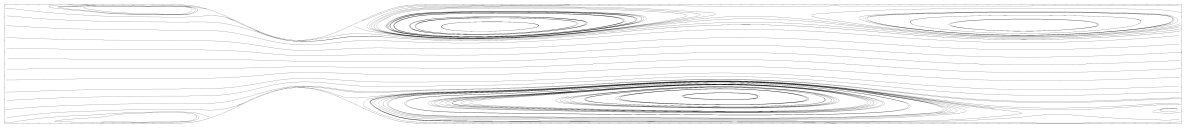

(c) t/T = 0.40

(d) t/T = 0.60

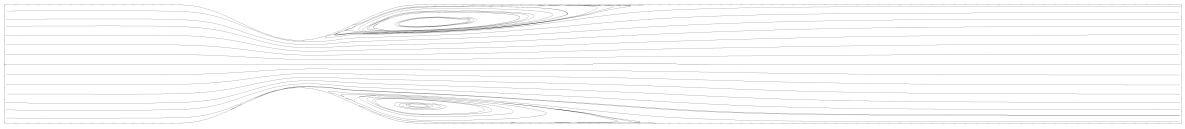

(e) t/T = 0.80

Figure 4.12: Snapshots of evenly distributed streamlines of the fluid over one period, under pulsatile inlet distibution described in Table 4.2

Granular population is then inserted, each grain hypothetically representing small aggregates of platelets. Snapshots of simulation results are shown in Figure 4.13. As previoulsy observed, particles are diffused following the area expansion, instead of travelling along the flow axis. Those particle are then entrapped within the building circulation zone, and will be mixed to the flow during the next pulse.

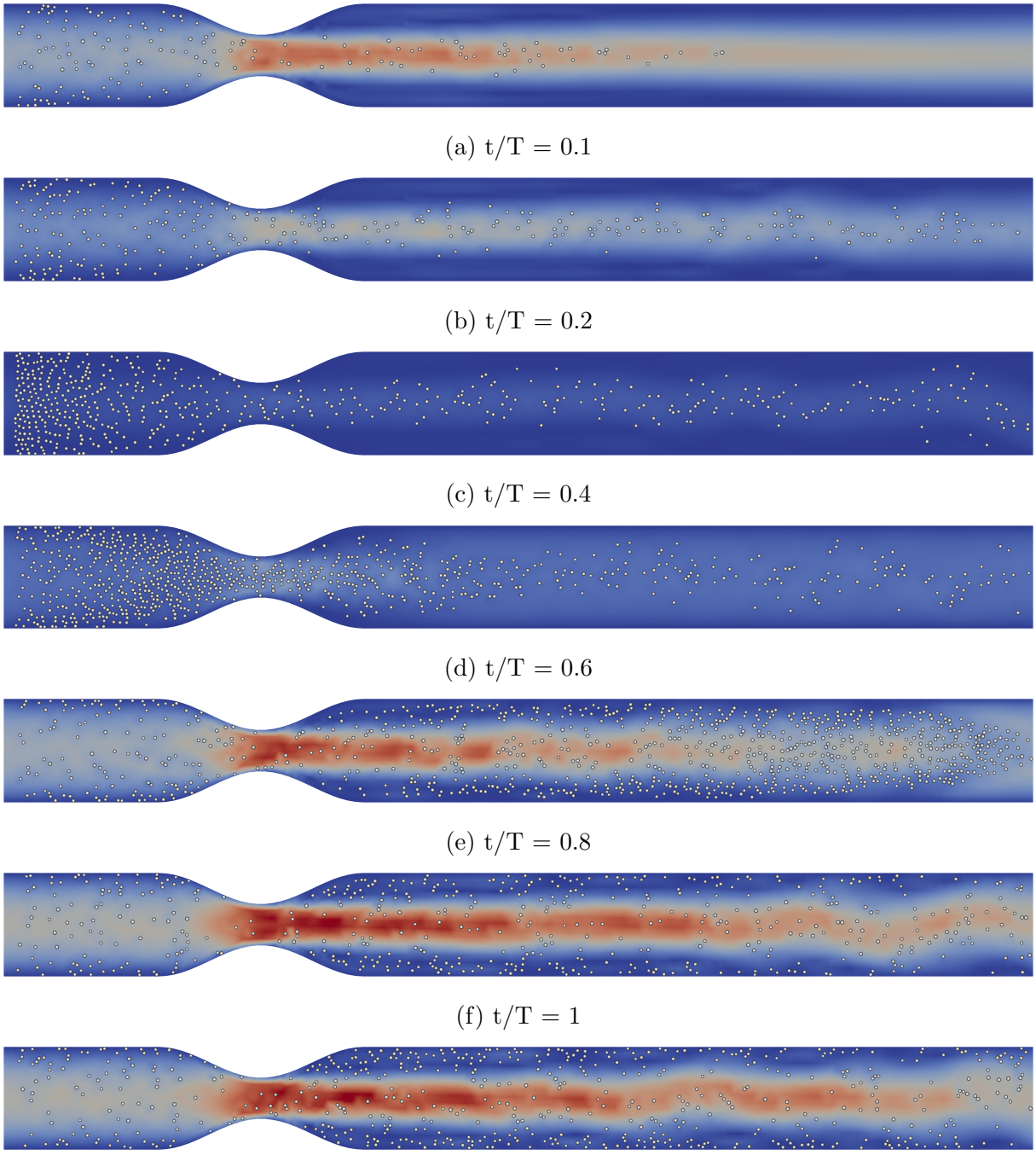

(a) t/T = 0.1

(b) t/T = 0.2

(c) t/T = 0.4

(d) t/T = 0.6

(e) t/T = 0.8

(f) t/T = 1

(g) t/T = 4

Figure 4.13: Simulation results for granular flow under pulsed conditions. Diffusivity of particle trajectories is observed in (d). (f) and (g) show symmetrical distribution and concentration of platelets.

4.2.4 Cohesion

The investigation of the blood flow behaviour through the stenosis and the effect of blood flow pulsation show great impact on platelet interaction and deposition. However, those

aspects are not sufficient to promote stable platelet deposition and aggregation. The study of these aspects is of primary importance because they suggest the importance of cohesive aspect of the particles within the flow. The cohesion described in the previous chapter is yet implemented in the stenosis case. The aggregation strategy is essentially the same as depicted in the thrombosis case, and is represented in figure 4.14. An initial population of fixed cohesive particles is set randomly at the stenosis wall, representing an injured area. The injury could result from a previous plaque rupture. Fixed particle radius are uniformly distributed $\sim \mathbf{U}(0.6, 1.2) \cdot r_p$, to provide heterogeneous geometric interactions and varying cohesive field force.

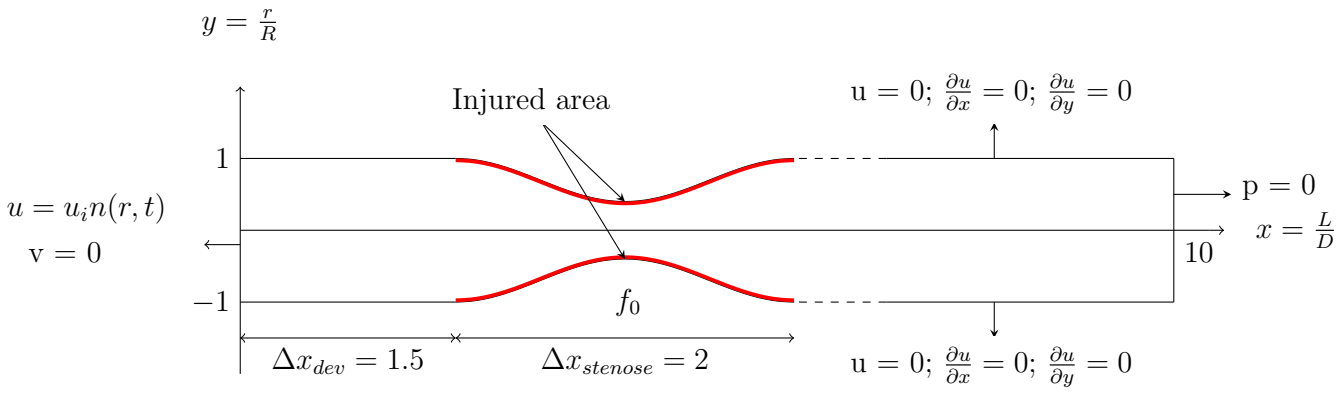

Figure 4.14: Stenose : problem conditions for simulation with cohesion

Since the scale of the experiment is raised to capture physical oscillatory phenomena (Womersley number is function of the vessel radius), particles are considered as platelets aggregates for relevance, since their relative low size to the vessel diameter would dramatically increase computational cost. Moreover, another empirical calibration is considered with calibration parameters $D_e = 10^{-6}[Nm]$. However, the naive calibration of the cohesion law leads to consider high calibration constant, that increases the stiffness of the problem and drives the method unstable as in the case of thrombosis. Attention is thus given to numerical computations: the time step is reduced as well as the number of particles. Figure 4.15 shows simulation results:

Platelet aggregates preferentially develop in the post stenosis region, where re-circulating zones promote smooth particle interaction. Clot extends the stenosis until becoming an active actor of the flow restriction. At this point, one understands that additional bounding factor between particles such as collagen or fibrin, would definitely stabilises the clot and avoid rupture as observed between Figure 4.15c and 4.15d.

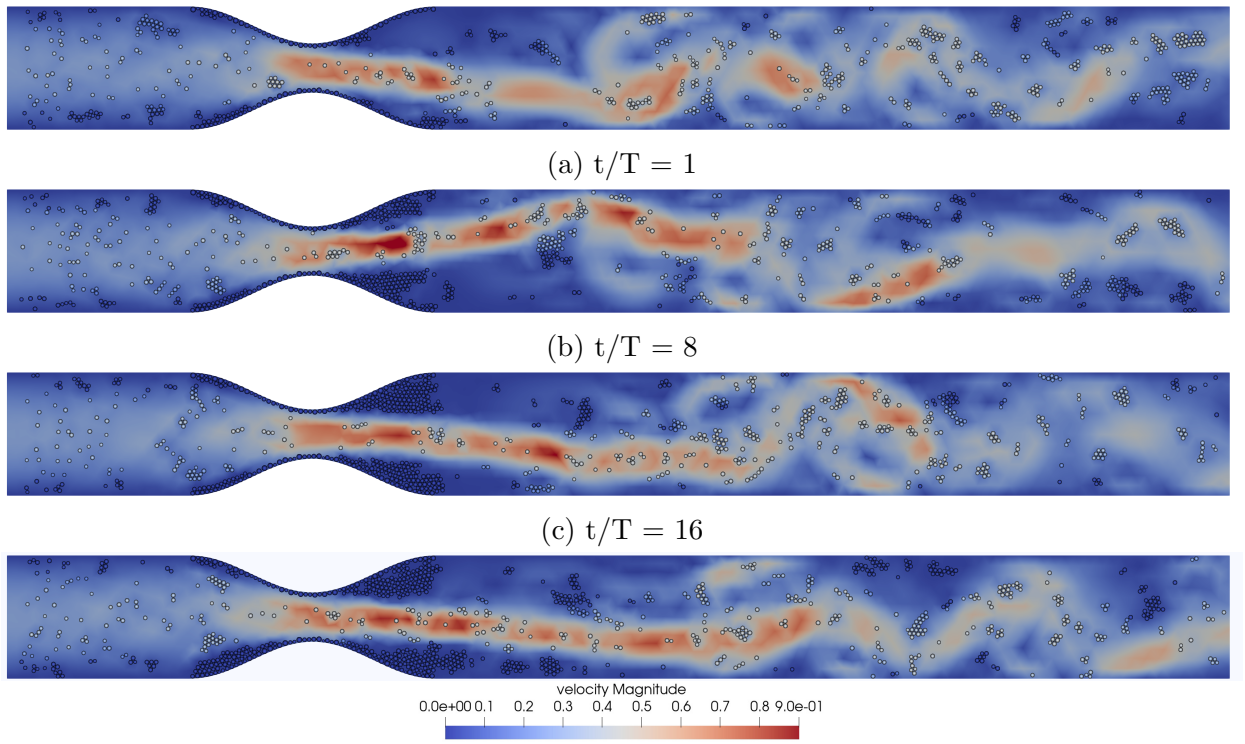

(a) t/T = 1

(b) t/T = 8

(c) t/T = 16

(d) t/T = 32

Figure 4.15: Simulation results for cohesive granular flow under pulsed inlet velocity condition. Every snapshot corresponds to maximum inlet pulse intensity. A color filter on the particle velocity improves visualisation of aggregated and immobilized particles (in dark blue). The calibration allows aggregated platelets to pack at the injury site and to form a clot.

4.3 Outcomes

This chapter study blood through an arterial stenosis. The flow is naively modeled as a suspension of adhesive particle representing blood platelets in an aqueous phase. Since plaque rupture is a major atherosclerotic events, the flow behaviour is investigated through a freshly ruptured stenosis, such that stenosis wall present cohesive properties. First the fluid is studied, and particular interest is dedicated to pulsed inlet velocity conditions that brings simulation results closer to reality. When considering granular suspension of particles, pulsed inlet speed profile also promotes presence and diffusion of platelets near the stenosis wall in the post-stenotic region due to the cyclic building of recirculating zones. This effect is particularly visible for dense particle suspension. For sake of providing a realitic representation of blood properties, the scale of the experiment is raised, providing coherent Womersley and Reynold numbers. Consequently, simulation particules are assumed to be aggregates of blood platelets. Finally, platelet cohesion and aggregation resulting in clot formation is observed along the injured area given an appropriate empirical calibration of the cohesive law.

Conclusion

Cardio-vascular disease prevention and treatments emphasize the need for accurate representation of blood flows. Atherosclerosis is recognized as the genesis of multiple cardio-vascular events. This thesis presented a first approach to understand the apparition of atherosclerosis, by representing blood flow as a dilute suspension of blood particles through the MigFlow software.

In the first chapter, blood components, their roles and their properties have been thoroughly described. It stressed that the particulate aspect of blood is at the origin of its rheological behaviour. A state of art presented the principal models used for blood representation. While continuous models are largely represented, reviewed discrete numericals methods which model blood flows at the scale of red blood cells seemed to better address blood description at a its particulate level. Since particle-particle and fluid-particle interaction description is key to the comprehension of the cardio-vascular events addressed in this thesis, the MigFlow software compared favourably to these methods. Within the scope of this master thesis one cannot consider the entire description of all blood species, and a simplified approach that focuses on a blood platelet population diluted in blood plasma was retained. This approach does not capture all the explicited rheological aspects of blood, nor does it model the bio-chemical interactions between particles. Yet, the usage of a multi-phasic representation still allows to partly capture the non Newtonian characteristics of the flow.

In the second chapter the Lagrangian-Eulerian architecture of the MigFlow software is described. Porosity is used to couple representations of the fluid and of the discrete particles. The solving of the contact resolution of colliding particles is obtained by the non smooth contact dynamics methods. One also observed that adding a cohesive contact law to the NSCD method is managable without altering its efficiency or adding complexity to its implementation.

In the third chapter, investigation of the underlying processes of hemostasis and coagulation identified blood platelets as major actors of coagulation whose disorders can lead to cariovascular occlusive event such as thrombus formation. One seeked to demonstrate the aggregation of platelets at a prescribed site of injury while submitted to a flow of cohesive platelets. Under pure granular approach (i.e. without fluid phase), vessel obstruction and clot formation could eventually be observed under empirical calibration of the cohesive law. Additional simulations including red blood cells described as a supplementary non cohesive particle population have also shown that cohesion could be maintained subject to significant increase of the cohesive properties of platelets. The fluid was then introduced in the simulations and one observed that the fluid inertia collapses the previously observed aggregation

patterns. By pushing the calibration of the cohesive law to more harsher levels, aggregative effects are recovered at the site of the injury. This tends to demonstrate the robustness of the implicit MigFlow method which allows proper flow conditions under stiffer calibration of the cohesive law. From a clinical perspective, the need to use such severe calibration to observe coagulation and thrombus formation seems to highlight the naive formulation of the problem. One have considered whether the shortfall could be mitigated when introducing other flow conditions that may favour platelets aggregation.

Fourth chapter provides a description of the initiation and evolution of the atherosclerosis, its principal physical manifestation of atherosclerosis is the formation of a stenosis, that locally modifies blood flow conditions and promotes platelets deposition. The impact of flow restriction and Reynolds number in an artery are firstly studied on the fluid phase with steady and pulsed inlet velocity profile. Different flow configuration are used to observe impact of the stenosis on the downstream flow. Variable re-circulations zones are obtained but an undesired flow asymmetry is observed, presumably linked to the 2D representation of the flow. Introducing a non cohesive platelet population, steady inlet profile was first analysed and showed some aggregation patterns. However, these seem mainly driven by the downstream conditions that progressively bring platelets back to stenosis region, while expectations would be that they directly migrate to the stenosis wall. The pulsatile approach, more representative of real conditions, revealed enhanced platelets diffusion in the vicinity of the vessel wall in the post stenotic region which is more in line with expectations. This analysis showed the influence of the flow inlet conditions on the trajectories and diffusion of blood platelets with potential impact on atheromous plaque growth. Adding cohesive properties to this pulsatile approach comforted the previous observations, and showed platelet aggregation at the wall. It is worth noting, that the need for representative arterial flow regarding Reynolds and Womerley number requires to raise the scale of the experiment.

The aim of this thesis was to evaluate the relevancy of a multiphase model to explain the apparition of atherosclerosis. This objective has been achieved with respect to the efficient modelisation of cohesive inter-particular interactions of blood platelets at particulate scale. This thesis is also a contribution to the MigFlow software with the integration of a cohesive law in the NSCD method. Simulation results show that coagulation and aggregation can be obtained subject to stiff empirical calibration. This might suggest that the formulation of the problem does not capture all the underlying physics. Clot stabilisation through fibrine polymerisation would require further exploration and experimentally based calibration. Morphological transformation of activated platelets could also be integrated in the formulation of the cohesion model. Yet managing deformability of cells contradicts with the assumptions of the implemented NSCD method.

Bibliography

M Anand and Kr Rajagopal. A shear-thinning viscoelastic blood model for describing the flow of blood. *Int. J. Cardiovascular Medicine and Science*, 4, January 2004.

M. Anand, J. Kwack, and A. Masud. A new generalized Oldroyd-B model for blood flow in complex geometries. *International Journal of Engineering Science*, 72:78–88, November 2013.

T. B. Anderson and Roy Jackson. Fluid Mechanical Description of Fluidized Beds. Equations of Motion. *Ind. Eng. Chem. Fund.*, 6(4):527–539, November 1967. Publisher: American Chemical Society.

N Anitschkow and S Chalatow. On experimental cholesterol steatosis and its significance in the development of various pathologic processes. page 1:9, 1913.

Alex J. Apostolidis and Antony N. Beris. Modeling of the blood rheology in steady-state shear flows. *Journal of Rheology*, 58(3):607–633, May 2014. Publisher: The Society of Rheology.

Nicola Begent and G. V. R. Born. Growth Rate in vivo of Platelet Thrombi, produced by Iontophoresis of ADP, as a Function of Mean Blood Flow Velocity. *Nature*, 227(5261): 926–930, August 1970. Number: 5261 Publisher: Nature Publishing Group.

John C. Chapin and Katherine A. Hajjar. Fibrinolysis and the control of blood coagulation. *Blood Rev*, 29(1):17–24, January 2015.

Shiyi Chen and Gary D. Doolen. Lattice Boltzmann Method for Fluid Flows. *Annual Review of Fluid Mechanics*, 30(1):329–364, 1998.

S. Chien. Shear dependence of effective cell volume as a determinant of blood viscosity. *Science*, 168(3934):977–979, May 1970.

Y. I. Cho and K. R. Kensey. Effects of the non-Newtonian viscosity of blood on flows in a diseased arterial vessel. Part 1: Steady flows. *Biorheology*, 28(3-4):241–262, 1991.

Matthieu Constant, Frédéric Dubois, Jonathan Lambrechts, and Vincent Legat. Implementation of an unresolved stabilised FEM–DEM model to solve immersed granular flows. *Computational Particle Mechanics*, 6, September 2018.

P. A. Cundall and O. D. L. Strack. A discrete numerical model for granular assemblies. *Géotechnique*, 29(1):47–65, March 1979. Publisher: ICE Publishing.

Mary Cushman. Epidemiology and Risk Factors for Venous Thrombosis. *Semin Hematol*, 44 (2):62–69, April 2007.

Sandro De Gruttola, Kevin Boomsma, and Dimos Poulikakos. Computational Simulation of a Non-Newtonian Model of the Blood Separation Process. *Artificial Organs*, 29(12): 949–959, 2005.

Eugene C. Eckstein, Arno W. Tilles, and Frank J. Millero. Conditions for the occurrence of large near-wall excesses of small particles during blood flow. *Microvascular Research*, 36 (1):31–39, July 1988.

Robin Fåhraeus. The suspension stability of the blood. *Physiological Reviews*, 9(2):241–274, April 1929. Publisher: American Physiological Society.

Robin Fåhræus and Torsten Lindqvist. The viscosity of the blood in narrow capillary tubes. *American Journal of Physiology-Legacy Content*, 96(3):562–568, March 1931. Publisher: American Physiological Society.

Dmitry A. Fedosov, Hiroshi Noguchi, and Gerhard Gompper. Multiscale modeling of blood flow: from single cells to blood rheology. *Biomech Model Mechanobiol*, 13(2):239–258, April 2014.

A. Fogelson and R. Guy. Immersed-boundary-type models of intravascular platelet aggregation*. 2008.

Aaron L Fogelson. A mathematical model and numerical method for studying platelet adhesion and aggregation during blood clotting. *Journal of Computational Physics*, 56(1): 111–134, October 1984.

Aaron L. Fogelson. Continuum Models of Platelet Aggregation: Formulation and Mechanical Properties. *SIAM Journal on Applied Mathematics*, 52(4):1089–1110, 1992. Publisher: Society for Industrial and Applied Mathematics.

Yuan-Cheng Fung. *Biomechanics*. Springer New York, New York, NY, 1993.

Bruce Furie and Barbara C. Furie. Mechanisms of thrombus formation. *N Engl J Med*, 359 (9):938–949, August 2008.

R. A. Gingold and J. J. Monaghan. Smoothed particle hydrodynamics: theory and application to non-spherical stars. *Monthly Notices of the Royal Astronomical Society*, 181(3): 375–389, December 1977.

Brian Haines and A. Mazzucato. A Proof of Einstein's Effective Viscosity for a Dilute Suspension of Spheres. *SIAM Journal on Mathematical Analysis*, 44, April 2011.

Z. Hashemi. Chapter 22 - The Lattice Boltzmann Modeling: Solving Complex Flows Including Biological Cells. In Miguel Cerrolaza, Sandra J. Shefelbine, and Diego Garzón-Alvarado, editors, *Numerical Methods and Advanced Simulation in Biomechanics and Biological Processes*, pages 391–414. Academic Press, January 2018.

P. J. Hoogerbrugge and J. M. V. A. Koelman. Simulating Microscopic Hydrodynamic Phenomena with Dissipative Particle Dynamics. *EPL*, 19(3):155–160, June 1992. Publisher: IOP Publishing.

S. Majid Hosseini and James J. Feng. A particle-based model for the transport of erythrocytes in capillaries. *Chemical Engineering Science*, 64(22):4488–4497, November 2009.

Seok In and In Seok Kang. A microscopic study on the rheological properties of human blood in low concentration limit. *Korea-Australia rheology journal*, 14, June 2002.

M. Jean. The non-smooth contact dynamics method. *Computer Methods in Applied Mechanics and Engineering*, 177(3):235–257, July 1999.

Hiroki Kamada, Ken-ichi Tsubota, Masanori Nakamura, Shigeo Wada, Takuji Ishikawa, and Takami Yamaguchi. A three-dimensional particle simulation of the formation and collapse of a primary thrombus. *International Journal for Numerical Methods in Biomedical Engineering*, 26(3-4):488–500, 2010.

D. N. Ku, D. P. Giddens, C. K. Zarins, and S. Glagov. Pulsatile flow and atherosclerosis in the human carotid bifurcation. Positive correlation between plaque location and low oscillating shear stress. *Arteriosclerosis*, 5(3):293–302, June 1985.

Karin Leiderman and Aaron L. Fogelson. Grow with the flow: a spatial–temporal model of platelet deposition and blood coagulation under flow. *Mathematical Medicine and Biology: A Journal of the IMA*, 28(1):47–84, March 2011.

Karin Leiderman and Aaron L. Fogelson. The Influence of Hindered Transport on the Development of Platelet Thrombi Under Flow. *Bull Math Biol*, 75(8):1255–1283, August 2013.

D. Liepsch and S. Moravec. Pulsatile flow of non-Newtonian fluid in distensible models of human arteries. *Biorheology*, 21(4):571–586, 1984.

L. B. Lucy. A numerical approach to the testing of the fission hypothesis. *The Astronomical Journal*, 82:1013–1024, December 1977. ADS Bibcode: 1977AJ.....82.1013L.

Daisuke Mori, Koichiro Yano, Ken-Ichi Tsubota, Takuji Ishikawa, Shigeo Wada, and Takami Yamaguchi. Simulation of platelet adhesion and aggregation regulated by fibrinogen and von Willebrand factor. *Thromb Haemost*, 99(1):108–115, January 2008.

Rajinder Pal. Rheology of concentrated suspensions of deformable elastic particles such as human erythrocytes. *Journal of Biomechanics*, 36(7):981–989, July 2003.

E. Marc Parmentier, William A. Morton, and Harry E. Petschek. Platelet aggregate formation in a region of separated blood flow. *The Physics of Fluids*, 20(12):2012–2021, December 1977. Publisher: American Institute of Physics.

Charles S. Peskin. Flow patterns around heart valves: A numerical method. *Journal of Computational Physics*, 10(2):252–271, October 1972.

Ronald J. Phillips, Robert C. Armstrong, Robert A. Brown, Alan L. Graham, and James R. Abbott. A constitutive equation for concentrated suspensions that accounts for shear-induced particle migration. *Physics of Fluids A: Fluid Dynamics*, 4(1):30–40, January 1992. Publisher: American Institute of Physics.

Igor V. Pivkin, Peter D. Richardson, and George Karniadakis. Blood flow velocity effects and role of activation delay time on growth and form of platelet thrombi. *Proc Natl Acad Sci U S A*, 103(46):17164–17169, November 2006.

Morayma Reyes Gil. Chapter 91 - Overview of the Coagulation System. In Beth H. Shaz, Christopher D. Hillyer, and Morayma Reyes Gil, editors, *Transfusion Medicine and Hemostasis (Third Edition)*, pages 559–564. Elsevier, January 2019.

R. Ross, J. Glomset, and L. Harker. Response to injury and atherogenesis. *Am J Pathol*, 86 (3):675–684, March 1977.

Russell Ross. Atherosclerosis — An Inflammatory Disease. *N Engl J Med*, 340(2):115–126, January 1999.

Getu Gamo Sagaro, Gopi Battineni, Marzio Di Canio, Andrea Minciacchi, Giulio Nittari, and Francesco Amenta. A descriptive epidemiological study of cardiovascular diseases among seafarers. *Int Marit Health*, 72(4):252–258, 2021.

Nobuatsu Tanaka and Tatsuo Takano. Microscopic-scale simulation of blood flow using sph method. *Int. J. Comput. Methods*, 02(04):555–568, December 2005. Publisher: World Scientific Publishing Co.

G. B. Thurston. Frequency and shear rate dependence of viscoelasticity of human blood. *Biorheology*, 10(3):375–381, September 1973.

A. Tosenberger, V. Salnikov, N. Bessonov, E. Babushkina, and V. Volpert. Particle Dynamics Methods of Blood Flow Simulations. *Math. Model. Nat. Phenom.*, 6(5):320–332, 2011. Number: 5 Publisher: EDP Sciences.

A. Tosenberger, F. Ataullakhanov, N. Bessonov, M. Panteleev, A. Tokarev, and V. Volpert. Modelling of thrombus growth in flow with a DPD-PDE method. *Journal of Theoretical Biology*, 337:30–41, November 2013.

Saji Varghese, Steven Frankel, and Paul Fischer. Direct numerical simulation of stenotic flows. Part 1. Steady flow. *Journal of Fluid Mechanics*, 582:253–280, July 2007.

Rudolph Virchow. Phlogose und Thrombose im Gefasssystem. *Gesammelte Abhandlungen zur Wissenschaftlichen Medicin*, page 458, 1856.

Frank Weichert, Lars Walczak, Denis Fisseler, Tobias Opfermann, Mudassar Razzaq, Raphael Münster, Stefan Turek, Iris Grunwald, Christian Roth, Christian Veith, and Mathias Wagner. Simulation of Intra-Aneurysmal Blood Flow by Different Numerical Methods. *Computational and Mathematical Methods in Medicine*, 2013:1–10, 2013.

John W. Weisel and Rustem I. Litvinov. Fibrin Formation, Structure and Properties. *Subcell Biochem*, 82:405–456, 2017.

J. R. Womersley. Method for the calculation of velocity, rate of flow and viscous drag in arteries when the pressure gradient is known. *The Journal of Physiology*, 127(3):553–563, 1955.

Zhiliang Xu, Nan Chen, Malgorzata M. Kamocka, Elliot D. Rosen, and Mark Alber. A multiscale model of thrombus development. *J R Soc Interface*, 5(24):705–722, July 2008.

Alireza Yazdani, He Li, Jay D. Humphrey, and George Em Karniadakis. A General Shear-Dependent Model for Thrombus Formation. *PLoS Comput Biol*, 13(1):e1005291, January 2017.

Junfeng Zhang, Paul C. Johnson, and Aleksander S. Popel. Red blood cell aggregation and dissociation in shear flows simulated by lattice Boltzmann method. *Journal of Biomechanics*, 41(1):47–55, January 2008.

UNIVERSITÉ CATHOLIQUE DE LOUVAIN
École polytechnique de Louvain
Rue Archimède, 1 bte L6.11.01, 1348 Louvain-la-Neuve, Belgique | **www.uclouvain.be/epl**